Graduate School ETD Form 9
(Revised 01/14)

PURDUE UNIVERSITY
GRADUATE SCHOOL
Thesis/Dissertation Acceptance

This is to certify that the thesis/dissertation prepared

By Anahita Emami

Entitled
Design Optimization of Heterogeneous Microstructured Materials

For the degree of Master of Science in Mechanical Engineering

Is approved by the final examining committee:

Andrés Tovar

Likun Zhu

Tamer Wasfy

To the best of my knowledge and as understood by the student in the *Thesis/Dissertation Agreement. Publication Delay, and Certification/Disclaimer (Graduate School Form 32)*, this thesis/dissertation adheres to the provisions of Purdue University's "Policy on Integrity in Research" and the use of copyrighted material.

Andrés Tovar

Approved by Major Professor(s): _____

_____

Approved by: Jie Chen 07/25/2014

Head of the Department Graduate Program Date

DESIGN OPTIMIZATION OF HETEROGENEOUS MICROSTRUCTURED MATERIALS

A Thesis
Submitted to the Faculty
of
Purdue University
by
Anahita Emami

In Partial Fulfillment of the
Requirements for the Degree
of
Master of Science in Mechanical Engineering

August 2014
Purdue University
Indianapolis, Indiana

ACKNOWLEDGEMENTS

First and foremost, I would like to thank my advisor, Professor Andrés Tovar, for his guidance, encouragement, support, and patience during the entire course of this work. I consider it a privilege to have worked with him and I will always be grateful for the substantial part he has played in my education. This research has been partially supported by the Air Force Office of Scientific Research, AFOSR FA9550-09-0633, Program Manager: Dr. Ali Sayir. I would also like to thank the members of my committee, Professor Tamer Wasfy and Professor Likun Zhu for serving on my thesis committee and for their valuable comments. Through their instruction, they have both provided me with an invaluable source of knowledge during my master study.

Moreover, I would like to take this opportunity to thank the entire team of Engineering Design Research Laboratory with whom I had the opportunity to work: Tong Wu, Kunal Khadhe, Satyajeet Sinde, Ashish Khanna, Kai Liu, and Josh Israel. It has been a pleasure to work with them all.

In Addition, I am indebted to Jafari family for helping, trusting, and supporting me during these two years. I might not have the opportunity to study at IUPUI without supporting of the Jafaris Fellowship program created through the generosity of Dr. Ali Jafari and his wife Mrs. Maymanat Montaser.

At last but not least, my further gratitude goes to my parents and family who supported and motivated me through all my life. I am also grateful to Meysam who has been with me during all ups and downs of my challenging journey and hopefully continues to be with me during all ups and downs on our way to come.

TABLE OF CONTENTS

Page

Page

LIST OF TABLES

LIST OF FIGURES

Figure Page

Figure Page

ABSTRACT

Emami, Anahita. M.S.M.E., Purdue University, August 2014. Design Optimization of Heterogeneous Microstructured Materials. Major Professor: Andrés Tovar.

Our ability to engineer materials is limited by our capacity to tailor the material's microstructure morphology and predict resulting properties. The insufficient knowledge on microstructure-property relationship is due to complexity and randomness in all materials at different scales. The objective of this research is to establish a design optimization methodology for microstructured materials. The material design problem is stated as finding the optimum microstructure to maximize the desired performance satisfying material processing constrains. This problem has been solved in this thesis by means of numerical techniques through four main steps: microstructure characterization, model reconstruction, property evaluation, and optimization. Two methods of microstructure characterizations have been investigated along with the advantages and disadvantages of each method. The first microstructure characterization method is a statistical method which utilizes correlation functions to extract the microstructural information. Algorithms for calculating these correlations functions have been developed and optimized based on their computational cost using MATLAB software. The second microstructure characterization method is physical characterization which works based on evaluation of physical features in microstructured domain. These features have been measured by means of MATLAB codes. Three model reconstruction techniques are proposed based on these characterization methods and employed to generate material models for further evaluation. The first reconstructing algorithm uses statistical functions to reconstruct the statistical equivalent model through simulating annealing optimization method. The second algorithm uses cellular automaton concepts to simulate the grain

growth utilizing physical descriptors, and the third one generates elliptical inclusions in a material matrix using physical characteristic of microstructure. The finite element method is used to analysis the mechanical behavior of material models. Several material samples with different microstructural characteristics have been generated to model the micro-scale design domain of AZ31 magnesium alloy and magnesium matrix composite with silicon carbide fibers. Then, surrogate models have been created based on these samples to approximate the entire design domain and demonstrate the sensitivity of the desired mechanical property to two independent microstructural features. Finally, the optimum microstructure characteristics of material samples for fracture strength maximization have been obtained.

1. INTRODUCTION

1.1. Justification

The continuing technological advancement strongly relies on our ability as engineers to design and develop new products that meet increasingly ambitious requirements. However, the quality of a product designed by a mechanical engineer is limited by the properties of available materials since the design process typically stops at the part level rather than the material level of the product system hierarchy shown in Figure 1.1. Then, materials are selected based on available material property charts, but they are not designed. Hence, the performance of many engineered products is limited by the properties of available constituent materials. For example, the demand of light-weight materials in industry has brought the attention of engineers to magnesium alloys which also possess many other desired mechanical properties such as high specific strength, high machinability, and fatigue resistance [1]. However, these alloys are inferior to the aluminum alloys in terms of toughness and fracture resistance. This fact is true in most cases that the combinations of all the desired properties are not available in typical material database.

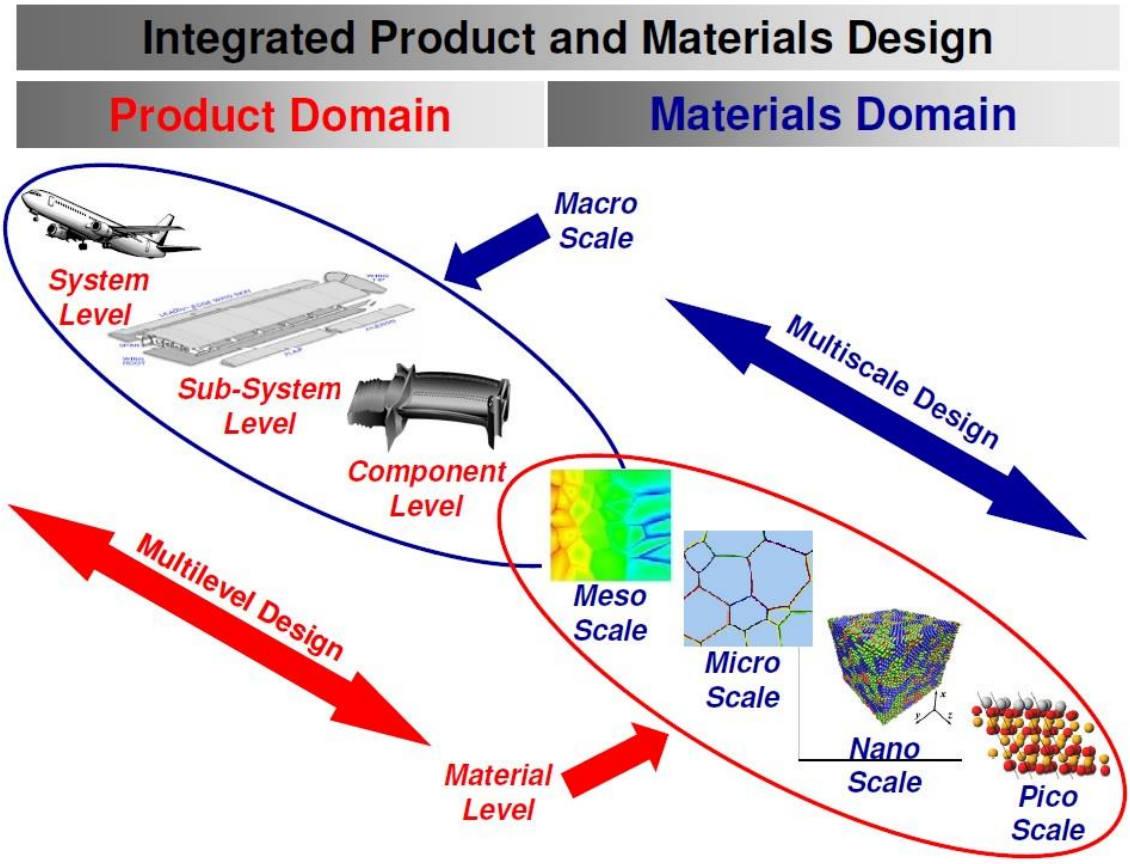

Figure 1.1. Hierarchical schematic of material design paradigm [2]

The development of new materials follows the traditional empirical approach of trial and error [2]. Repeated experiments in this approach are very expensive and time-consuming. Therefore, recent efforts have been devoted to tailoring material structure at various scales from nanoscale up to continuum level for specific product applications via a broad range of material-modeling tools. The main challenge in this course is to obtain knowledge of material structure-property relations that significantly affects system concepts for function-based, systematic design of product and material concepts in an integrated fashion [3], and the presence of randomness in different scale-levels has a significant role in complicating this challenge. Hence, currently understanding the influence of microstructural configurations on the bulk properties of materials is a critical demand in the field of material design.

1.2. State of the Art

1.2.1. Material by Design

Material design is an emerging multidisciplinary field in which both science-based tools and engineering systems design methods are utilized to tailor material structures and processing paths to achieve targeted properties, performance, and functionality for specific applications [4]. In traditional approaches, new materials have been developed with empirical, trial-and-error techniques and the experimental results have created material databases which can be utilized as a resource of material selection in a typical design approach. Therefore, the design process is limited to the selection of appropriate materials from the finite set of available material databases. In addition, lead times for the new materials development have remained expensive corresponding to product development cycles for new products [5]. Selection methods of materials from available databases have been proposed by Ashby [6]. These methods have been classified as selection by analysis, synthesis, similarity, or inspiration [7, 8]. Material selection methods are crucial for mapping materials' properties to their behaviors and performances, but the difficulty with material selection is due to the incapability of tailoring a material that perfectly accomplishes all the desired performances. Required combinations of properties might simply not be available from materials in current databases. Materials with various mechanical, thermal, electrical, and chemical properties have been grouped by Koller [9] in charts. Alternatively graphical representative forms of engineering and natural materials clustered based on their properties have been proposed by Ashby [6] as shown in Figure 1.2. Both Ashby and Koller established a classification scheme of properties for a variety of materials such as metals, alloys, composites, ceramics, and polymers.

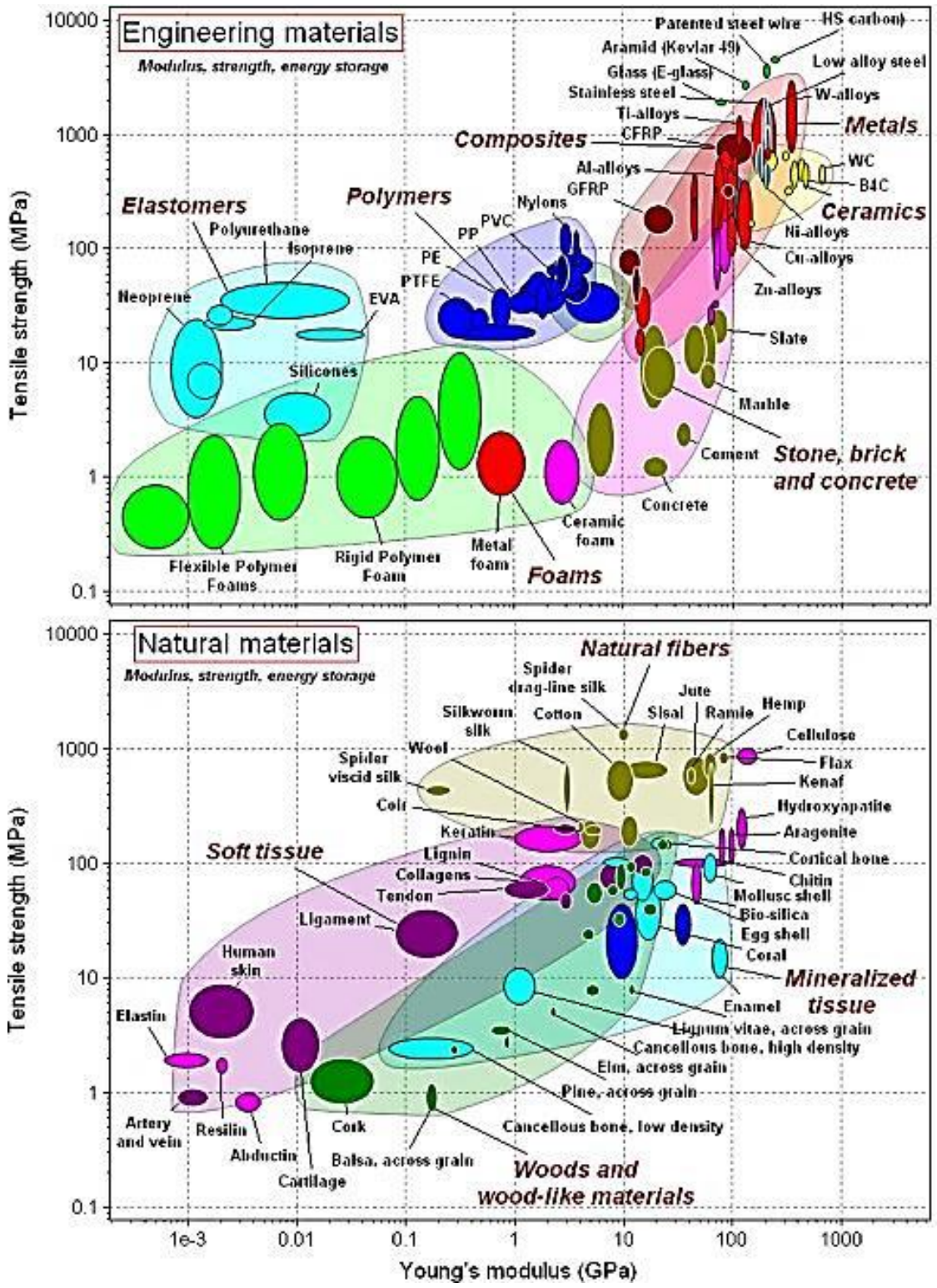

Figure 1.2. Ashby plot illustrating the Young's modulus and tensile strength of traditional engineering materials and natural materials on the same axis [7]

Besides the development of advanced methodologies for material selection, a paradigm shift towards materials design with the objective of tailoring the chemical composition, constituent phases, microstructure and processing paths to obtain materials with desired properties for specific applications has begun [4, 10-12].

Thus far, most existing techniques for materials design are mainly focused on developing multiscale modeling [12, 13] by means of computational techniques. This computational design synthesis includes four steps: representation, generation, evaluation, and guidance [14]. Although computational techniques are utilized to facilitate this new design approach of material synthesizing , but Eberhart and Clougherty [15] mentioned that regardless of how fast the computer, if it needs to search for an optimum property using accurate analysis models of an infinite number of materials, it will require infinite time to perform the search. Therefore, the perspective of materials design as an automated search is very limited. Nonetheless, complex models might not be necessary in many cases because the objective of materials design is not to accurately predict material properties but to satisfy performance requirements. Simple models can be developed to demonstrate sensitivity of material performance to its representative parameters.

A hierarchical framework of materials by design has been proposed by O'Sullivan [10] as shown in Figure 1.3. In this framework, the materials design challenge is to develop methods that employ bottom-up modeling and simulation, calibrated and validated by characterization and measurement, which also allow top-down exploration of the hierarchy of material scales. The inductive or deductive mappings that are necessary to support materials design according to this framework contains of following elements [4]:

- Process-structure relations that are used to establish manufacturing constraints, cost factors, thermodynamic and kinetic feasibilities of process routes.

- Structure-property relations between composition, phase and mesoscopic morphology and response functions or properties of relevance to desire performance attribute.
- Property-performance relations between properties and response functions and imposed performance requirements.

Since the understanding of structure-property relations is a core element of this framework that demands lots of investigations, this study focuses mainly on this part.

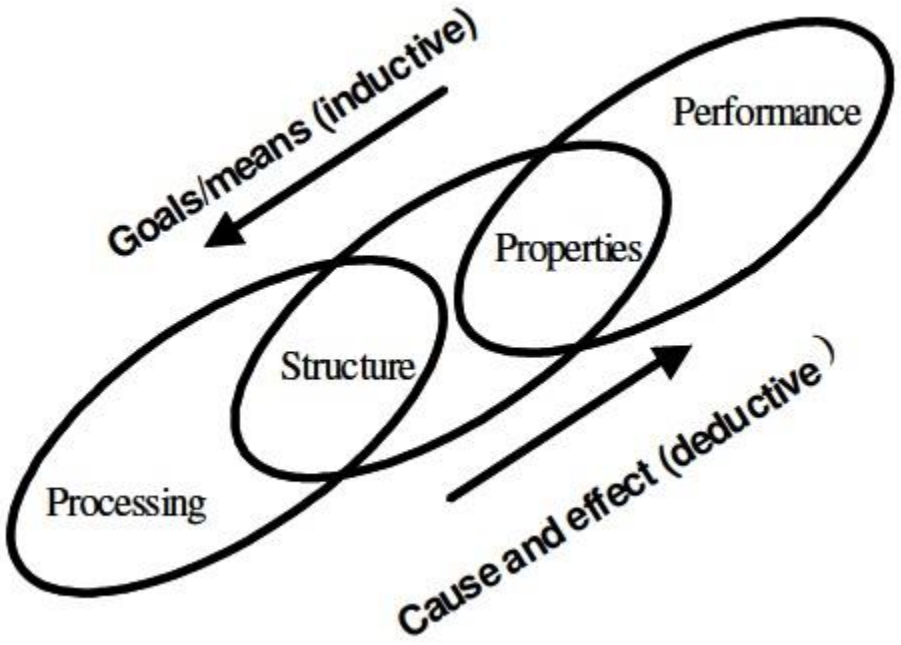

Figure 1.3. Olson's hierarchical framework of materials by design [11]

1.2.2. Heterogeneous Materials

A heterogeneous material is a material that is composed of domains of different materials or phases, such as a composite, or the same material in different states, such as a polycrystal [16]. As in many cases, the microstructures can just be characterized statistically, and they are categorized as random heterogeneous materials. Figure 1.4 depicts examples of scanning electron microscopic (SEM) of some heterogeneous

microstructured materials found in nature such as elk antler (a) and human dentin (b) or in synthetic material domain such as magnesium alloy (c) and magnesium matrix composite (d).

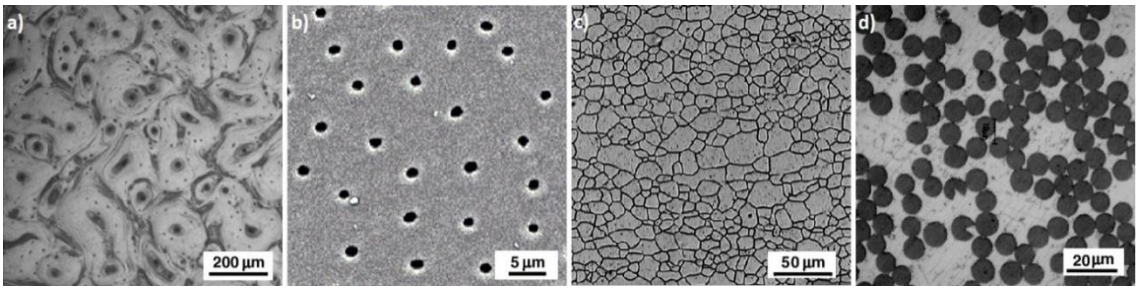

Figure 1.4. SEM images of sample heterogeneous microstructured materials: (a) transverse image of elk antler [18], (b) human dentin [19], (c) magnesium alloy [20], and (d) magnesium matrix composite [21]

The design of heterogeneous materials with optimal mechanical properties has attracted attention of many engineers and scientists [17-19]. The heterogeneous materials can be either made of random media in which any sample is a realization of specific random or stochastic process, or follows a distinguishable pattern like periodic media. Nevertheless, in any types of heterogeneous materials, the effective properties such as average elastic moduli, thermal conductivity, and viscosity among others, depend on phases' properties and microstructural information, including volume fractions of different phases, which represent the simplest level of information. In most cases, the material properties are not simply related to the volume fractions of different phases. They generally depend on complex interactions between different phases and nontrivial features of microstructures. For example, the Voigt model [20], which is the arithmetic weighted average of the phase properties, is the exact evaluation of effective property of parallel layered composites when the applied field is in the parallel direction of the layers (as shown in Figure 1.5.a). This formula can just give an overestimation of the effective property for other composition of materials, especially when the phases have broadly different properties. Therefore, Equation (1.1) just gives the upper bound of effective mechanical properties such as elastic modulus here (E_e), for general two phase materials

in which φ_1 and φ_2 are volume fractions of phase one and two with elastic modulus of E_1 and E_2 respectively.

$$E_e = E_1\varphi_1 + E_2\varphi_2 \tag{1.1}$$

On the other hand, the Reuss model [21] which is the harmonic average of the phase properties and the exact evaluation of effective property of parallel layered composites when the applied field is in the perpendicular direction of the layers (as shown in Figure 1.5.b) gives an underestimation of the effective property for other type of composite materials. Consequently, Equation (1.2) gives the lower bound of effective mechanical properties for two phase materials.

$$E_e = \left(\frac{\varphi_1}{E_1} + \frac{\varphi_2}{E_2}\right)^{-1} \tag{1.2}$$

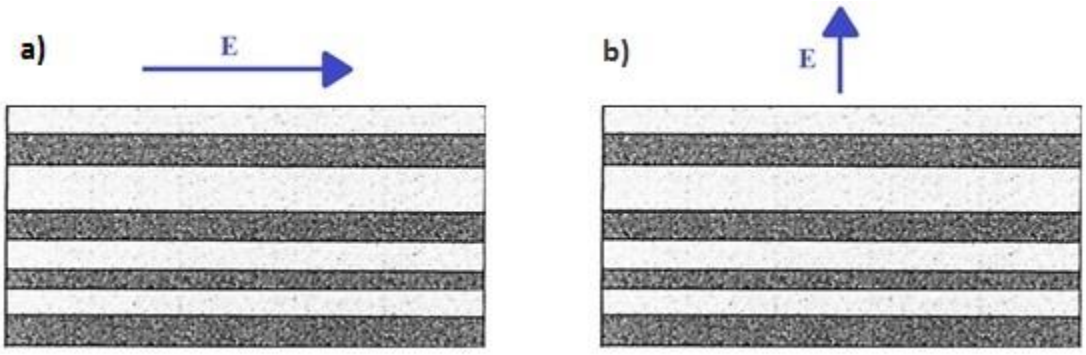

Figure 1.5. (a) Two-phase layered composite under parallel applies field and (b) two-phase layered composite under perpendicular applies field

As an illustration of a sample microstructural feature other than phase volume fractions that has significant influence on effective properties, consider a 50-50 two-phase system as shown in Figure 1.6.a. which consists of disconnected inclusion phase and a connected matrix phase. Material shown in Figure 1.6.b has exactly the same microstructure but with interchanged phases. Assuming the red phase has any specific higher mechanical property such as fracture strength, thermal conductivity, or elastic modulus, than the green phase. It is obvious that the material system with red matrix has effective higher properties than the other one, which means the property of connected

phase, dominate the effective properties of the whole material system. This fact is shown by trend of crack propagation through these two examples. As it can be observed when the grains are more brittle than matrix the initial vertical crack propagate through the grains, but when the matrix is more brittle the crack propagates along the grains boundaries and not through them.

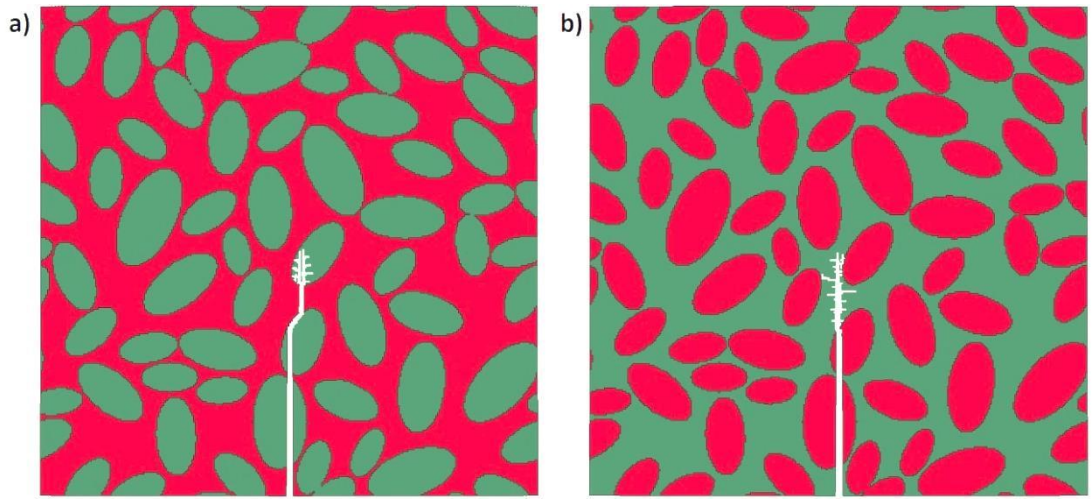

Figure 1.6. Crack propagation trend in 50-50 two-phase material systems with the same morphology but interchanged phases

Therefore, both composites with the same volume fraction can have completely different effective mechanical properties. In other words, the effective properties of a system depend on microstructural information beyond the volume fractions of its components. Other microstructural features that govern the effective mechanical properties include surface area of interfaces, shapes, sizes, orientations, and spatial distribution of inclusions among others.

1.2.3. Quantification of Microstructured Materials

The quantification of microstructured materials refers to identification of proper parameters that can represent microstructural features in accordance with their actual contributions to the material property and performance. The origin of this approach can be found in several classical works. For example, the effective elastic properties of a solid

with spherical pores on the basis of individual pore contributions to the overall compliance were studied by Mackenzie in 1950 [22]. Then, the isotropic matrixes of polycrystals consisting of anisotropic inhomogeneities of spherical crystals were studied by Koner in 1958 [23]. He investigated the effect of a single crystal on the bulk elasticity behavior of polycrystals. In 1965 Hill [24] explored ellipsoidal inhomogeneities and evaluated their contributions to the overall elasticity using Eshelby's results [25, 26] A review of many elementary works done in this field was published by Markov [27]. In spite of all these efforts, the relations between many microscale features and macroscale properties have not been discovered yet. Specifically when the material possesses a highly random microstructure, it becomes more difficult to quantify the proper microstructural features that affect the bulk material behavior.

Information-complexity profile of materials is demonstrated in Figure 1.7. A complexity profile counts the number of independent effects at a specific scale and contains the effects that have impact at larger scales. The use of the term complexity reflects a quantitative theory of the degree of difficulty in describing the behavior of a system. This theory simply counts the number of independent effects as a measure of the complexity of a system or amount of information available. Thus, the complexity profile characterizes system behaviors by describing the complexity as a function of scale, and it increases exponentially as the scale lowers. For instance, the material's structure at nano-scale contains much more information than at micro-scale which indicates more flexibility in design at lower scales. Currently extracting all this information seems infeasible. Even in micro-scale the structural information can be so convoluted that it is impossible to quantify the information properly. However, this microstructural information is essential in material design practice. In this study, some data-mining approaches of microstructures are first introduced. Then, they are utilized to generate a model for material property analysis.

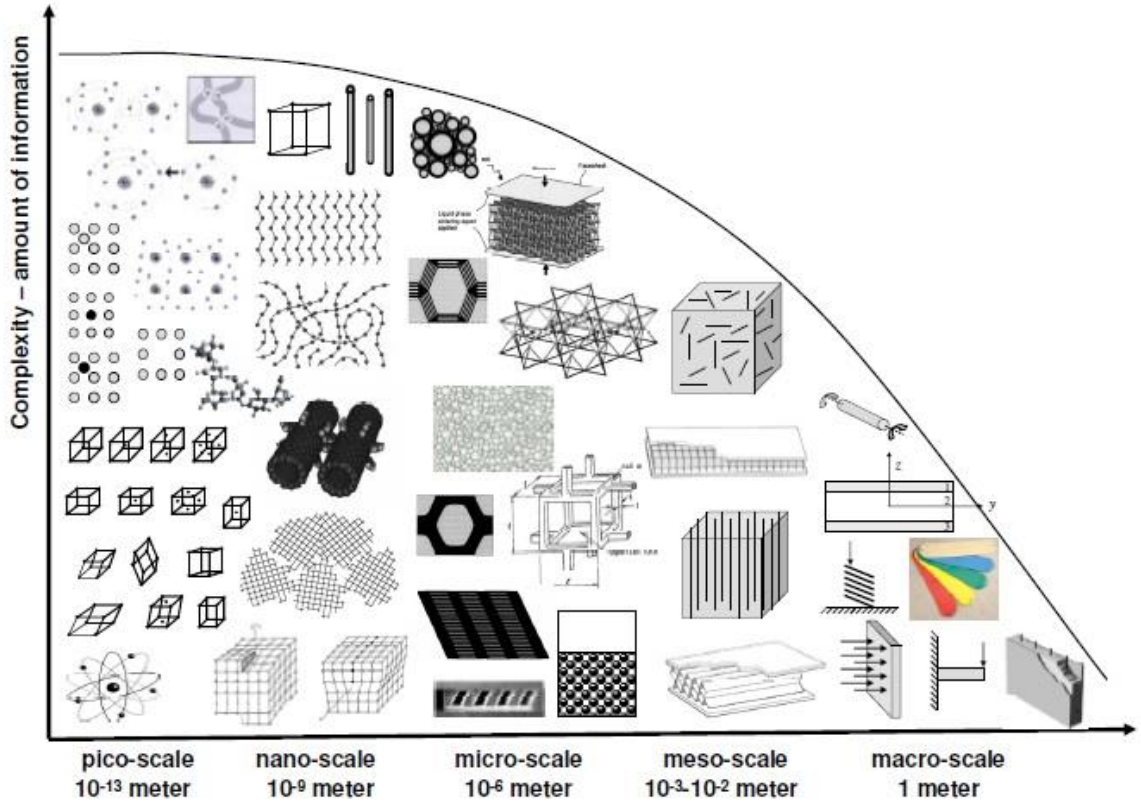

Figure 1.7. Complexity of quantification at different material scales [33]

1.3. Objective

The main objective of this research is to optimize heterogeneous material performance through material design framework focusing on the material's microstructure. This goal is achieved in four steps. The first step is representation of micro-scale domain through statistical or physical-based characterization techniques as explained in Chapter 2. Different descriptors are required to extract the microstructural information lying under the morphological configuration of a material's microstructure. After representation of microstructural domain, this information is utilized in the second step for reconstruction of equivalent microstructure or generation of a model which contains the same micro-scale information as the actual material. The fidelity of the generated model mainly depends on the amount of information conveyed by

characteristic parameters which are utilized in the reconstructing algorithms. These algorithms are explained in Chapter 3.

In the third step after model generation, the desired mechanical behavior is evaluated by the finite element method. These three steps provide the elements required to solve the main material optimization problem. The descriptors conveying microstructural information, which are obtained in the first step, are treated as the optimization variables, and the maximization of fracture strength is the objective function of the optimization problem. The model generated in the second step is a link between the optimization variables and the objective function. The final step is called guidance which is the optimization approach selected for solving this problem. Since the search domain is infinite, the surrogate model-based optimization is employed to solve the problem. In this approach, the behavior of objective function is estimated based on the value of the function for sample variables, which can give a reasonable approximation of the optimal material behavior in accordance with certain microstructural features.

1.4. Original Contributions

Simulation-based design framework was first introduced by Olson [28]. In the present thesis, statistical and physical-based characterization and reconstruction approaches are incorporated in this framework to establish the material design methodology. First, algorithms for evaluation of statistical correlation functions in any type of two-phase materials have been developed. These algorithms are superior in terms of accuracy and computational cost to the Monte Carlo technique. In addition, several physical features of microstructured material have been extracted by means of MATLAB codes. These features serve as the input parameters of model-reconstructing algorithms. Consequently, three different reconstruction algorithms have been developed. The first one is based on statistical characteristics and the simulated annealing optimization method. The two others incorporate physical features to reconstruct a material model using cellular automaton principles and non-overlapping elliptical inclusion generation

respectively. Finally, a surrogate model-based approach has been proposed for material optimization. This method utilizes finite number of sample points in the variable domain to estimate the behavior of the correspondence function over the entire domain by interpolation methods.

2. MATERIAL CHARACTERIZATION

The main goal of material characterization is to obtain the morphological features of materials that have significant influence on the effective mechanical properties. In this study, the digital images of microstructures that captured by techniques such as scanning electron microscope (SEM) or transmission electron microscope (TEM) are utilized for computational characterization. Since the phase information of each pixel of these types of images is marked by a specific grey-scale value, image processing is needed to segment the images to prepare them for further characterization process. Moreover, existence of noise in digital images is inevitable, therefore appropriate filtering and quality enhancing algorithms are mandatory for de-noising and processing them. Thus, the image processing steps which are necessary to prepare an image for further characterization will be explained in the first section. Then, two different approaches of statistical and physical-based characterization will be presented in the second and third sections respectively. Finally in the last section, the comparison between two approaches will be discussed and the advantages and disadvantages of each approach will be explained.

2.1. Image Processing

One of the most challenging aspects of material characterization is image processing, since without a high quality and precise image of a microstructure no accurate information can be obtained. Thus, this step can be the major source of errors and uncertainties in the results, if it is not accomplished properly. In this study, image processing toolbox of MATLAB is mainly utilized to preprocessing the SEM or TEM images. This toolbox provides set of reference-standard algorithms and functions for

image enhancement, noise reduction, and image segmentation among other processing tools.

2.1.1. Filtering

Digital images are prone to variety types of noise which is the result of inevitable errors in the image acquisition process. As a result of noise presence in the image, some pixel values do not reflect the true intensities of the real scene. Depending on the type of noise in a digital image, apposite filtering technique or combination of some techniques has to be implemented for noise reduction. In this section, a SEM image of magnesium alloy section as it is shown in Figure 2.1.a is selected as a sample to demonstrate different noise reduction techniques. The effect of three different techniques of contrast enhancement has been demonstrated in Figure 2.1.a-d for image correction.

In the first algorithm of image adjustment, the contrast of the image is increased by mapping the intensity values of the gray scaled pixels to new values such that, 1% of the data is saturated at low and high intensities of the input data. The resulted image is illustrated in Figure 2.1.b. As it is shown, this technique stretches the histogram of the image. In Figure 2.1.c, contrast enhancement technique using histogram equalization was applied to the original image. In this technique the contrast in the entire image has been enhanced by transforming the intensity values of pixels so that histogram of the image approximately matches a uniform distribution.

Alternatively, the other enhancement technique, called contrast-limited adaptive histogram equalization (CLAHE), operates on small data regions (tiles) rather than the entire image. In this technique, each tile's contrast is enhanced so that the histogram of each output region approximately matches the uniform distribution. In this technique, the contrast enhancement can be limited in order to avoid amplifying the noise which might be present in the image. The image and histogram resulted from this technique is

illustrated in Figure 2.1.d. This algorithm is mainly utilized when the illumination of the image is not uniform and the gradient illumination patterns cause noise in the image.

Although for this sample image, the adjustment technique just gives an acceptable filtered result but, some other sample images may need different type of filtering or a more complex algorithm with combination of different techniques. Therefore, the filtering technique is not unique and can be changed from one image to another.

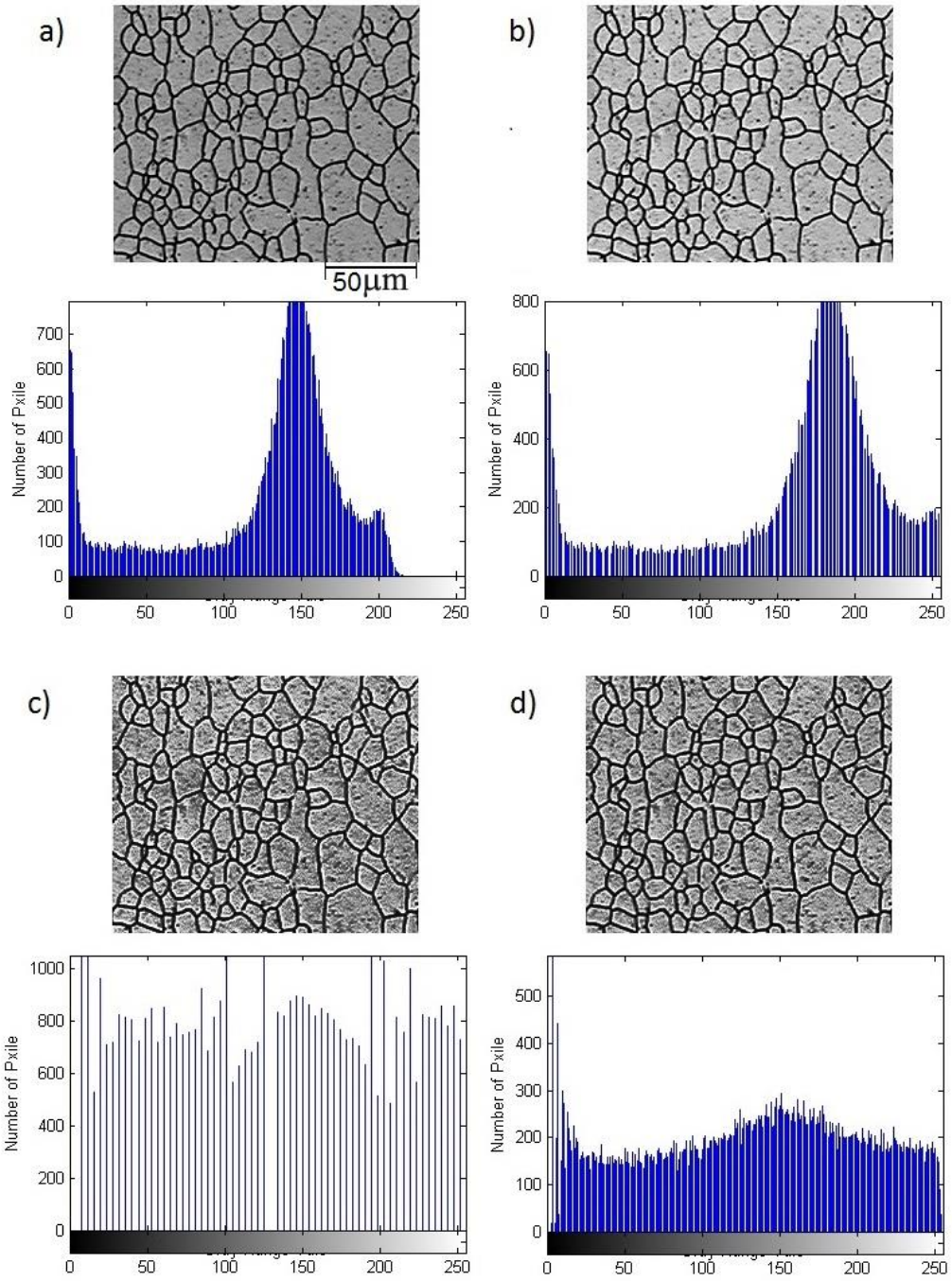

Figure 2.1. (a) Original SEM image, (b) image after adjustment technique by stretching the histogram, (c) image after histogram equalization technique, and (d) image after contrast-limited adaptive histogram equalization

2.1.2. Image Segmentation

Segmentation involves separating an image into regions corresponding to different phases of materials. The purpose of image segmentation is to distinguish information of each phase with high amount of accuracy. The simplest property that pixels in a specific phase in SEM or TEM gray-scaled image can share is intensity. Thus, the gray scale image of two-phase material must be converted to black and white based on the difference in light intensity that pixels of each phase possess. Sometimes, it is required to sharpen an image to intensify the difference between two phases and be able to identify the border of each face precisely. However, the problem with sharpening is that if the noise in the image has not been eliminated completely it will be intensified by this approach. Therefore, further filtering may be needed to eliminate the intensified noise before converting to black and white image.

When the image has been pre-processed and become ready for segmentation, the major challenge in converting the gray scale image to black and white image (binary image) is specifying the correct threshold level. Thresholding creates binary images by turning all pixels below some threshold level to zero (black) and all pixels above that to one (white). However, if intensity is only considered without involving any relationships between the pixels, there is no guarantee that the pixels identified by the thresholding process are contiguous. It is likely to miss isolated pixels within the region, especially near the boundaries of the region or include extraneous pixels that aren't part of the phase of interest. This effect can be also worsened by presence of noise in the image. Another problem with global thresholding is that changes in illumination across the image may cause some regions to be brighter and some darker in ways that have nothing to do with the material phases. This problem of uneven illumination can be partially solved by determining thresholds locally to smoothly vary across the image. One of the well-established clustering-based image thresholding to compute the threshold level is Otsu's method [29] which chooses the threshold to minimize the intra-class variance of the black and white pixels. Although, this method can give a good approximation of threshold level for the image, but still it may be needed to adjust this threshold level to correct it for a

specific image. The black and white result of segmentation after elimination most of the noises in the image is shown in Figure 2.2 on the right side of the initial image.

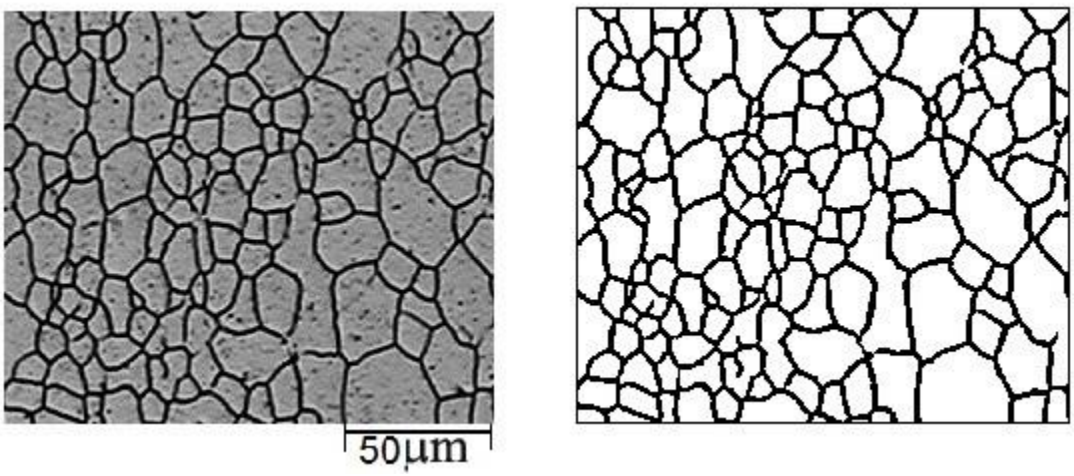

Figure 2.2. Left: the original image before any processing. Right: the final black and white image after processing and segmentation.

2.2. Statistical Characterization

A random two-phase microstructure medium can be regarded as a probability space that can be characterized with statistical approaches [30]. Many descriptors have been proposed for quantification of heterogeneous microstructure [16, 31, 32]. However, correlation functions are the most popular ones that have been used to characterize many different heterogeneous media. Torquato [16] defined the following microstructural correlation functions as the fundamental to determining the effective properties of random heterogeneous materials:

1) N-point correlation function
2) Surface correlation functions
3) Lineal- path function
4) Chord-length density function
5) Pore-size functions
6) Percolation and cluster functions
7) Nearest-neighbor functions

The six correlation functions at the first of the list, which are referred as general correlation functions in this dissertation, can be applied to describe any random media with arbitrary microstructures, but the last one in the list can just be used to describe random media with spherical particles.

In this article, the correlation functions for two-phase media will be introduced, but it can be extended in similar way for multiple-phase media as well. Before giving the precise definition of these correlation functions, some basic terms should be defined here. Considering a volume of two-phase material, each phase occupies a volume subset V_i for $i = 1,2$ and the volume containing the microstructure (V) is partitioned disjoint phases with volume fractions Φ_i for $i = 1,2$. Then, the indicator function $I^{(i)}(\vec{x})$ for a random variable at coordinate $\vec{x} \in V$, is defined by [18]:

$$I^{(i)}(\vec{x}) = \begin{cases} 1, & \text{if } \vec{x} \in V_i\,, \quad (i = 1,2) \\ 0, & \text{otherwise.} \end{cases} \tag{2.1}$$

Therefore, the $I^{(1)}(\vec{x}) + I^{(2)}(\vec{x}) = 1$ is valid for any $\vec{x} \in V$ in two phase material systems or in general case $\sum_{i=1}^{n} I^{(i)}(\boldsymbol{x}) = 1$ is true for n phase material systems. Additionally, the indicator function $M(\mathbf{x})$ for the interface is defined as:

$$M(\vec{x}) = \left|\nabla I^{(1)}(\vec{x})\right| = \left|\nabla I^{(2)}(\vec{x})\right| \tag{2.2}$$

This function is nonzero when $\vec{x}$ is located on the interface of two phase. Assuming a fixed point at $\vec{x}$, the indicator function $I^{(i)}(\vec{x})$ can just have two possible values: 0 or 1 (excluding the Dirac delta functions). Hence, the random variable $I^{(i)}(\vec{x})$ does not have a probability density function.

2.2.1. N-point Probability Function

The n-point probability function, also called n-point correlation function, is defined as probability of finding n point at positions $\vec{x}_1, \vec{x}_2, \ldots, \vec{x}_n$ in the phase of interest.

Therefore, when *n* is equal to one this probability function can be expressed as the probability that $I^{(i)}(x)$ equals one which is written as:

$$S_1^{(i)}(\vec{\boldsymbol{x}}) = P\{I^{(i)}(\vec{\boldsymbol{x}}) = 1\} = \langle I^{(i)}(\vec{\boldsymbol{x}})\rangle \tag{2.3}$$

Where the angular brackets denote an ensemble average, which is defined as an average over all realizations of the ensemble. An ensemble is a collection of all the possible realization of a random medium generated by a specific stochastic process. This one point probability function generally is equal to volume fraction of phase of interest Φ_i. Similarly the n-point probability function can be written as:

$$\begin{aligned} S_n^{(i)}(\vec{\boldsymbol{x}}_1, \vec{\boldsymbol{x}}_2, \dots, \vec{\boldsymbol{x}}_n) &= P\{I^{(i)}(\vec{\boldsymbol{x}}_1) = 1, I^{(i)}(\vec{\boldsymbol{x}}_2) = 1, \dots, I^{(i)}(\vec{\boldsymbol{x}}_n) = 1\} \\ &= \langle I^{(i)}(\vec{\boldsymbol{x}}_1) I^{(i)}(\vec{\boldsymbol{x}}_2) \dots I^{(i)}(\vec{\boldsymbol{x}}_n)\rangle \end{aligned} \tag{2.4}$$

Since in the two phase materials, it is true that $I^{(2)}(x) = 1 - I^{(1)}(x)$, the n-point probability function of one phase, e.g. phase 1, can be expressed in terms of phase 2 probability functions as following equation:

$$\begin{aligned} S_n^{(1)}(\vec{\boldsymbol{x}}_1, \vec{\boldsymbol{x}}_2, \dots, \vec{\boldsymbol{x}}_n) &= \langle \prod_{j=1}^{n} I^{(1)}(\vec{\boldsymbol{x}}_j)\rangle = \langle \prod_{j=1}^{n} [1 - I^{(2)}(\vec{\boldsymbol{x}}_j)]\rangle \\ &= 1 - \sum_{j=1}^{n} S_1^{(2)}(\vec{\boldsymbol{x}}_j) + \sum_{j<k}^{n} S_2^{(2)}(\vec{\boldsymbol{x}}_j, \vec{\boldsymbol{x}}_k) - \sum_{j<k<l}^{n} S_3^{(2)}(\vec{\boldsymbol{x}}_j, \vec{\boldsymbol{x}}_k, \vec{\boldsymbol{x}}_l) \\ &+ \dots + (-1)^n S_n^{(2)}(\boldsymbol{x}_1, \boldsymbol{x}_2, \dots, \boldsymbol{x}_n) \end{aligned} \tag{2.5}$$

In the same way the two point probability of two dissimilar ends $S_2^{(12)}(\vec{\boldsymbol{x}}_1, \vec{\boldsymbol{x}}_2)$ that a point at $\vec{\boldsymbol{x}}_1$ is located in phase 1 and a point at $\vec{\boldsymbol{x}}_2$ is located in phase 2 can be expressed in terms of one of each phase probability function as:

$$S_2^{(12)}(\vec{\boldsymbol{x}}_1, \vec{\boldsymbol{x}}_2) = \langle I^{(1)}(\vec{\boldsymbol{x}}_1)[1 - I^{(1)}(\vec{\boldsymbol{x}}_2)\rangle = S_1^{(1)}(\vec{\boldsymbol{x}}_1) - S_2^{(1)}(\vec{\boldsymbol{x}}_1, \vec{\boldsymbol{x}}_2) \tag{2.6}$$

Based on the concept of the statistical n-point correlation functions, random microstructured materials can be categorized into following classes:

Statistical inhomogeneous materials: a material system is called statistically inhomogeneous, if the n-point probability function $S_n^{(i)}(\vec{x}_1, \vec{x}_2, \dots, \vec{x}_n)$ depends generally on the absolute positions $\vec{x}_1$, $\vec{x}_2$, ..., $\vec{x}_n$,. Narrowing it to one point correlation function, it can be shown that volume fraction of phase of interest is position dependent. The microstructures of functionally graded materials are generally placed in this class. As shown in Figure 2.3, the volume fraction of particles increases leftward.

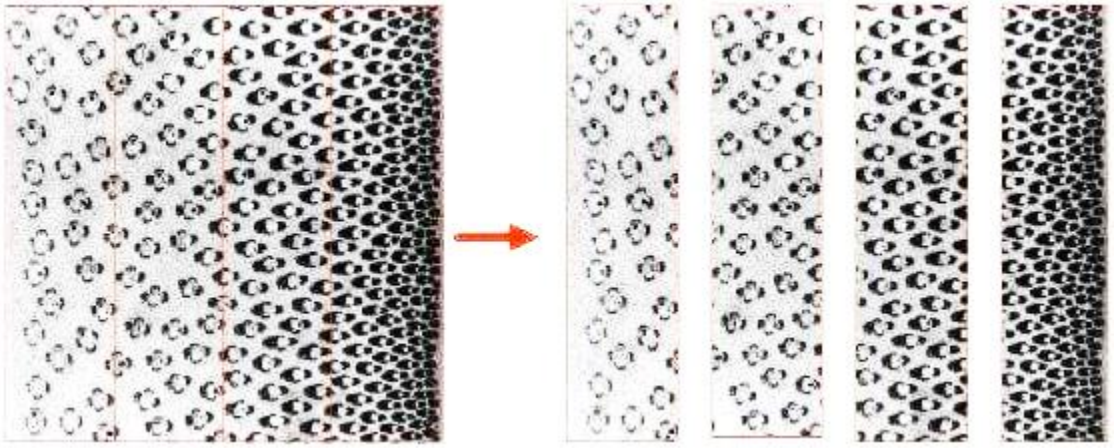

Figure 2.3. Example of statistically inhomogeneous material, sectioning the medium, the volume fraction of particles in each section significantly differs from the other sections [38]

Strictly statically homogeneous materials: a material system is called strictly statistically homogeneous if n-point probability function does not change by translation or shift of the original coordinate system. This implies that n-point correlation function is not dependent on the absolute positions but on relative displacements. This concept for all $n \geq 1$, $\vec{x}_j$ $(j = 1 \text{ to } n)$, and shift vector $\vec{y}$ in R^d can be shown in the following equation in which $\vec{r}_{jk} = \vec{x}_k - \vec{x}_j$:

$$S_n^{(i)}(\vec{x}_1, \vec{x}_2, \dots, \vec{x}_n) = S_n^{(i)}(\vec{x}_1 + \vec{y}, \vec{x}_2 + \vec{y}, \dots, \vec{x}_n + \vec{y}) = S_n^{(i)}(\vec{r}_{12}, \vec{r}_{13}, \dots, \vec{r}_{1n}) \tag{2.7}$$

Following this concept, it can be inferred that the one-point probability function is a constant everywhere which equals to volume fraction of phase of interest Φ_i. In other

words, the volume fractions are position-independent in this class of microstructured materials.

Statically homogeneous but anisotropic materials: a homogeneous material system is called anisotropic if the n-point probability function depends on both orientations and magnitudes of the vectors $\vec{\boldsymbol{x}}_1, \vec{\boldsymbol{x}}_2, \ldots, \vec{\boldsymbol{x}}_n$. A sample of anisotropic medium is demonstrated in Figure 2.4.a verses an isotropic medium in Figure 2.4.b.

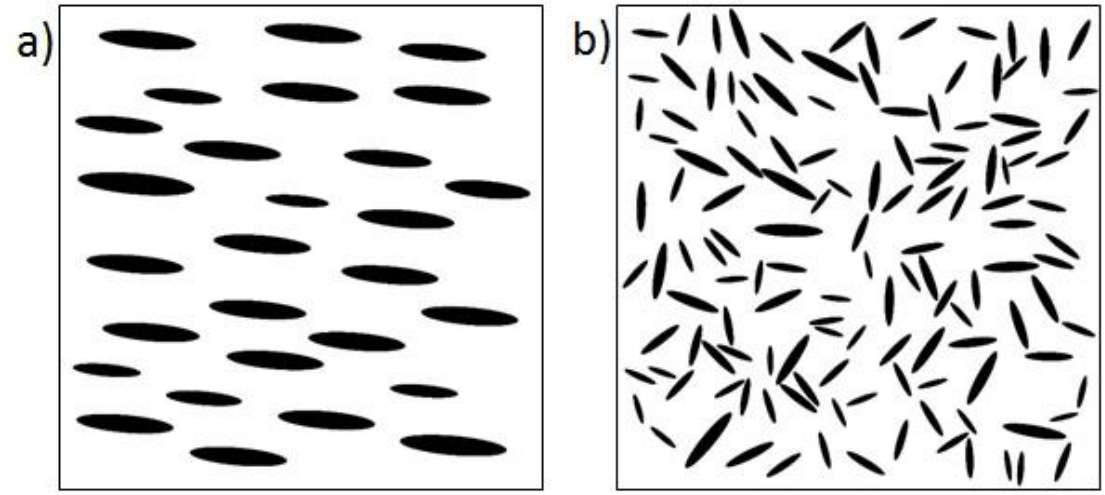

Figure 2.4. (a) Statistical anisotropic medium vs. (b) strictly statically isotropic medium

Strictly statically isotropic materials: a homogeneous material system is called statically isotropic if n-point probability function does not change by rotation of the original coordinate system. This means that n-point correlation function just depends on the scalar distances between points: $r_{jk} = \left|\vec{\boldsymbol{r}}_{\boldsymbol{jk}}\right|$, $1 \leq j \leq k \leq n$ and the following equation is valid:

$$S_n^{(i)}(\vec{\boldsymbol{x}}_1, \vec{\boldsymbol{x}}_2, \ldots, \vec{\boldsymbol{x}}_n) = S_n^{(i)}(\boldsymbol{r}_{12}, \boldsymbol{r}_{13}, \ldots, \boldsymbol{r}_{1n}) \tag{2.8}$$

A major property of statistically homogeneous microstructures is ergodicity which implies that complete probabilistic information can be evaluated from a single realization of the infinite medium. Providing the homogeneous microstructure is also isotropic, the *k* dimensional n-point correlation functions $(n \leq k)$ can be obtained from a

k-1 dimensional realization of the medium as long as the realization has large enough size to encompass all the information of higher order dimension. [16]

The upper boundary limit of n-point probability function can be generally obtained when all the *n* random points selected in the medium locate at the same position, which is equivalent to the probability of finding one point in the phase of interest. Henceforth, the maximum value that n-point probability function can obtain equals the volume fraction of phase of interest. It can be shown as following equation:

$$\lim_{\substack{\forall \vec{r}_{jk} \to 0 \\ 1 \le j \le k \le n}} S_n^{(i)}(\vec{x}_1, \vec{x}_2, \dots, \vec{x}_n) = S_1^{(i)}(\vec{x}_1) = \Phi_i \tag{2.9}$$

The lower boundary limit of n-point probability function will be obtained when all the *n* points selected as far as possible from each other (with infinite mutual displacement). In the absent of long-range order, which is discussed in the next paragraph, the events of *n* points with infinite mutual displacement occurs independently for all the points in a system. Therefore, the n-point correlation function for such a system can be written as the products of ensemble average of indicator function for all the subsets of set of points with infinity distances. For example, the *n*-point correlation function for one of the possible partitions of the set ($\vec{x}_1$, $\vec{x}_2$, ..., $\vec{x}_n$) can be written as follow:

$$\begin{aligned} &\lim_{\substack{\forall \vec{r}_{jk} \to \infty \\ 1 \le j \le k \le n}} S_n^{(i)}(\vec{x}_1, \vec{x}_2, \dots, \vec{x}_n) \\ &\qquad = \langle I^{(i)}(\vec{x}_1)\rangle \langle I^{(i)}(\vec{x}_2) I^{(i)}(\vec{x}_3)\rangle \langle I^{(i)}(\vec{x}_4) I^{(i)}(\vec{x}_5) I^{(i)}(\vec{x}_6)\rangle \dots \\ &\qquad = S_1^{(i)}(\vec{x}_1) S_2^{(i)}(\vec{x}_2, \vec{x}_3) S_3^{(i)}(\vec{x}_4, \vec{x}_5, \vec{x}_6) \dots \end{aligned} \tag{2.10}$$

A microstructured system possesses long-range order if there exist at least two points with statistically dependent infinite mutual displacement. For example, an infinitely large crystalline or periodic array of identical spheres as shown in Figure 2.5 possess long-range order, and its two-point correlation function has oscillatory behavior

and does not obey asymptotic results of Equation (2.10). On the other hand, the sample shown in Figure 2.6 does not have long-range order and its two-point correlation function approaches to its asymptotic value for large distance between two points.

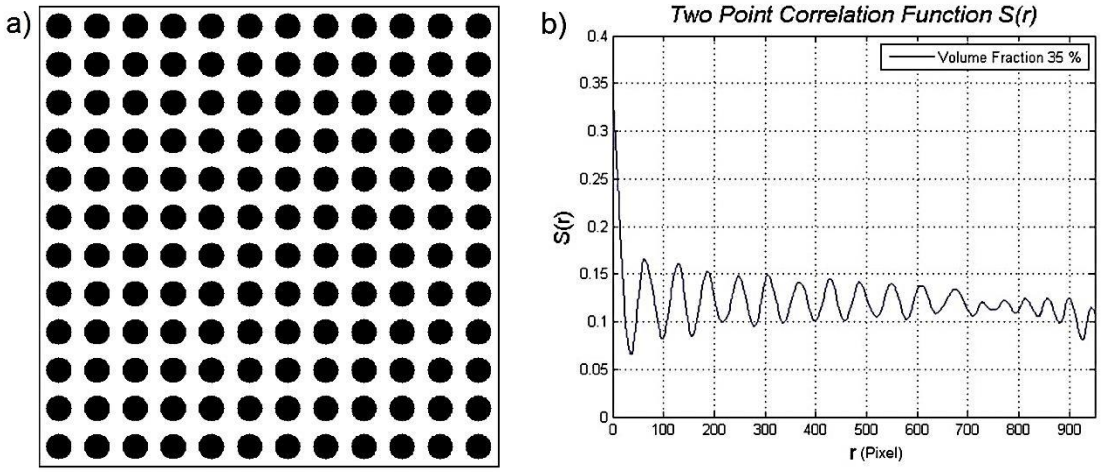

Figure 2.5. (a) A sample medium with long-range order and (b) plot of its two-point correlation function

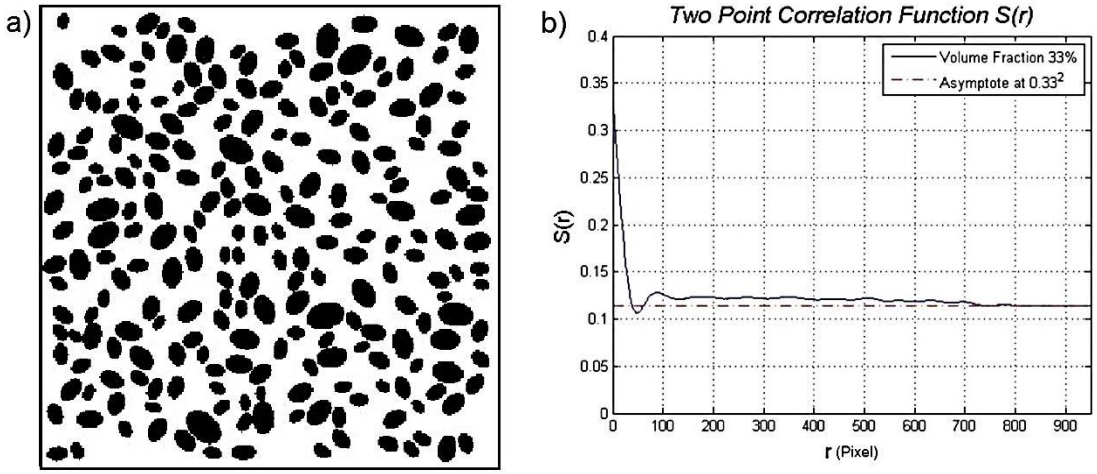

Figure 2.6. (a) A sample medium without long-range order and (b) plot of its two-point correlation function

Equation (2.10) for statistical homogeneous microstructure without long-range order results as following equation:

$$\lim_{\substack{\forall \vec{r}_{1j} \to \infty \\ j=2\ to\ n}} S_n^{(i)}(\vec{r}_{12}, \vec{r}_{13}, \dots, \vec{r}_{1n}) = (S_1^{(i)}(\vec{x}_1))^n = {\Phi_i}^n \tag{2.11}$$

As it is demonstrated in Figure 2.6, the two-point correlation function approaches its asymptotic value of squared volume fraction in the absence of long-range order.

2.2.1.1. Two-point Correlation Function

Since two-point correlation function is the lowest order *n*-point correlation function which includes microstructural information more than just volume fractions of different phases, it is well-accepted in practice. A fair amount of work on two-point correlation function characterization can be found in literature [33-44]. Based on the two-point correlation function definition, it can be depicted that just one out of four possible two-point correlation functions for a two-phase microstructure is independent and all three others are dependent by following relationships [45]:

$$S_2^{(1)}(\vec{x}_1, \vec{x}_2) + S_2^{(2)}(\vec{x}_1, \vec{x}_2) + S_2^{(12)}(\vec{x}_1, \vec{x}_2) + S_2^{(21)}(\vec{x}_1, \vec{x}_2) = 1 \tag{2.12}$$

$$S_2^{(12)}(\vec{x}_1, \vec{x}_2) = S_2^{(21)}(\vec{x}_1, \vec{x}_2) \tag{2.13}$$

$$S_2^{(1)}(\vec{x}_1, \vec{x}_2) + S_2^{(12)}(\vec{x}_1, \vec{x}_2) = \varphi_1 \tag{2.14}$$

Moreover, the derivative of two-point correlation function at the origin can be obtained from formula established by Debye et al. [46] for isotropic two-phase heterogeneous microstructures. It has been also shown by Berryman [47] that the formula is valid for anisotropic microstructure as well. As a result, the derivative of two-point correlation function at the origin for the first three *d*-dimensional spaces can be written as:

$$\left.\frac{dS_2^{(i)}}{dr}\right|_{r=0} = \begin{cases} -s/2\,, & d = 1 \\ -s/\pi\,, & d = 2 \\ -s/4\,, & d = 3 \end{cases} \tag{2.15}$$

Where *s* is the specific surface, defined as the interface area per unit volume. It has been also shown that the steepest descent of the two-point correlation function occurs at the origin [41]:

$$\left|\frac{dS_2^{(i)}}{dr}|_{r=0}\right| \geq \left|\frac{dS_2^{(i)}}{dr}|_{r>0}\right| \tag{2.16}$$

The convexity of two-point correlation function at the origin has been also represented as [40]:

$$\left|\frac{d^2S_2^{(i)}}{dr^2}|_{r=0}\right| \geq 0 \tag{2.17}$$

The approaches and algorithms for calculation of this correlation function are described in Section 2.2.8. The illustration for the event of this probability function in two phase material is also shown in Figure 2.9.

2.2.1.2. Three-point Correlation Function

It has been shown [48] that the two-point correlation function contains crucial but incomplete characterization of microstructures and it cannot completely specify a two-phase heterogeneous material alone, apart from the issue of chirality. Furthermore, different microstructures may have the same two point correlation function. Therefore, three-point correlation function as a higher order correlation function can be used as higher order characterization function for microstructures. This function is the probability of finding three points at locations $\vec{x}_1$, $\vec{x}_2$, and $\vec{x}_3$ in phase *i*. Similar to two-point correlation function, the thee-point correlation function is only related to scalar distance between the selected points in statistically homogeneous media [16]. Therefore, $S_3^{(i)}(\vec{x}_1, \vec{x}_2, \vec{x}_3) = S_3^{(i)}(r_{12}, r_{13})$ where $r_{12} = |\vec{x}_1 - \vec{x}_2|$ and $r_{13} = |\vec{x}_1 - \vec{x}_3|$. The value of three-point correlation function for both r_{12} and r_{13} equal zero shows the volume fraction of phase *i*. When only one of the distances is zero, which means two of the selected points are in the same position, the three-point correlation function is just related on the nonzero distance and it equals the two-point correlation function for that distance. In fact, three-point correlation function not only contains all the information of the lower order similar functions, but also more features information of microstructures. The contours of three point correlation function obtained for three different sample

compositions are shown in Figure 2.7 where r_1 and r_2 indicate r_{12} and r_{13} respectively. In sample (a) as it is shown in Figure 2.7, the structure has regular pattern with solid inclusions. In sample (b), inclusions have ring shape and the structure is not as regular as the first sample. However, sample (c) consists of just random shape inclusions. Comparing the results of three point correlation functions for these three types of compositions, it can be observed that symmetry exists in all the resulted contours. The highest value of the correlation function, as it was expected, can be found at the origin of the contour plot when three points are all selected in one position ($r_{12} = r_{13} = 0$). This value is the volume fraction of the inclusions. Moreover, the quantities at the horizontal and vertical axes, where r_{12} or r_{13} equals zero, represent the two point correlation function for the sample structures. The probability of finding three point in black phase decreases by increasing the distance values.

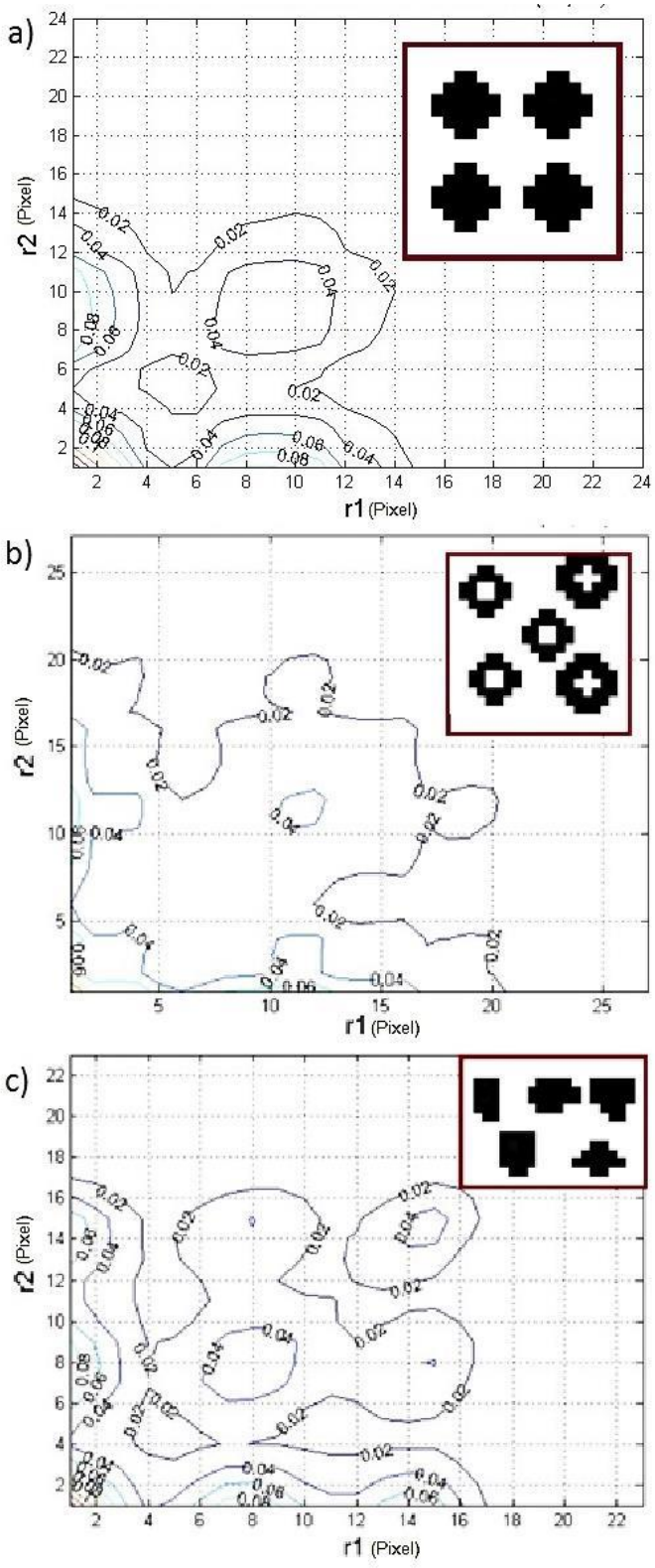

Figure 2.7. Three point correlation function for three sample media

2.2.2. Surface Correlation Functions

Surface correlation functions convey the information about the random interface, and it is not a probability function because the probability of finding a point on the interface in a continuum medium is zero. The simplest surface correlation function is the specific surface $s(\vec{x})$ defined as interface area per unit volume at point $\vec{x}$, which is a one-point correlation function with following equation:

$$s(\vec{x}) = \langle M(\vec{x}) \rangle \tag{2.18}$$

In homogeneous microstructure, the specific surface is a constant everywhere and can be simply denoted by s.

Similarly, two-point surface correlation functions are defined as:

$$F_{ss}(\vec{x}_1, \vec{x}_2) = \langle M(\vec{x}_1) M(\vec{x}_2) \rangle \tag{2.19}$$

$$F_{sv}(\vec{x}_1, \vec{x}_2) = \langle M(\vec{x}_1) I^{(v)}(\vec{x}_2) \rangle \tag{2.20}$$

Where s indicates the surface between two phases and v indicates inside phase v, and therefore $F_{sv}(\vec{x}_1, \vec{x}_2)$ represents the event that the point located at $\vec{x}_1$ lies on the interface of two phases and the point located at $\vec{x}_2$ lies inside the phase v. Since these functions have been originated from the trapping and flow problems of solid and void media [49-51], the phase v is usually considered as void phase. Therefore, F_{ss} and F_{sv} are called surface-surface and surface-void correlation functions respectively. The schematic of these events is depicted in Figure 2.9.

In homogeneous microstructure, these functions only depend on the displacement between two points ($\vec{r} = \vec{x}_2 - \vec{x}_1$), and when the material is statistically isotropic they depend on the distance between two points ($r = |\vec{r}|$). In microstructures without long-range order, when the distance between two points approaches infinity the two-point surface functions can be written as:

$$\lim_{r \to \infty} F_{ss}(r) = s^2 \tag{2.21}$$

$$\lim_{r \to \infty} F_{sv}(r) = s\varphi_v \tag{2.22}$$

Where φ_v is volume fraction of phase *v* or void phase. Similarly the *n*-point surface correlation functions can be defined. For example, surface-void correlation function with *m* points on the interface and *m*-*n* points inside the void phase can be defined by:

$$F_{ss\dots svv\dots v}(\vec{x}_1, \vec{x}_2, \dots, \vec{x}_m; \vec{x}_{m=1}, \dots, \vec{x}_n) = \left\langle \left[\prod_{i=1}^{m} M(\vec{x}_i) \right] \left[\prod_{j=m+1}^{n} I^{(v)}(\vec{x}_j) \right] \right\rangle \tag{2.23}$$

The application of surface correlation functions can be generally found where the interface area has an important role in mechanical properties of microstructure.

2.2.3. Lineal-path Function

Lineal-path function $L^{(i)}(r)$ was first introduced by Lu and Torquato [52] for strictly statically isotropic material as the probability that a line segment of specific length *r*, lands wholly in the phase of interest when randomly thrown into the microstructure. The schematic for the event of this probability function is depicted in Figure 2.9.

In statically homogeneous but anisotropic material, lineal-path function $L^{(i)}(\vec{r})$ depends on orientation of the line segment as well as its length, for that reason it is written as a function of vector $\vec{r}$. Furthermore for statistically inhomogeneous microstructures, lineal-path function $L^{(i)}(\vec{x}_1, \vec{x}_2)$ depends on absolute positions of the end points of the line segments $\vec{x}_1$ and $\vec{x}_2$.

This probability function contains useful statistical measures of phase connectivity, but just along a lineal path with specific length. This function is monotonically decreasing with respect to increase of line segment length, and the boundary values for this function is $L^{(i)}(0) = \varphi_i$ and $L^{(i)}(\infty) = 0$ where φ_i is the volume fraction of phase *i*. The behavior of this function at large length of line segment when it still has non-zero value contains information of the largest lineal path in the phase of

interest. The linear contact distribution function in the stochastic geometry has been also defined based on lineal-path function as the quantity of $\varphi_i (1 - L^{(i)}(r))$ [53].

In two phase strictly statically isotropic materials, $L^{(12)}(r)$ can be also defined as the probability of a line segment with length r which lands in both phases partially when randomly thrown into the media, thus the relationship between lineal path probability functions can be defined by:

$$L^{(1)}(r) + L^{(2)}(r) + L^{(12)}(r) = 1 \tag{2.24}$$

The plot of all three possible lineal path functions for two-phase isotropic media in presence and absence of long-range order as shown in Figure 2.5 and Figure 2.6 are depicted in Figure 2.8. In these plots, the inclusions (black phase) are denoted as phase 1, and the matrix (white phase) is denoted as phase 2.

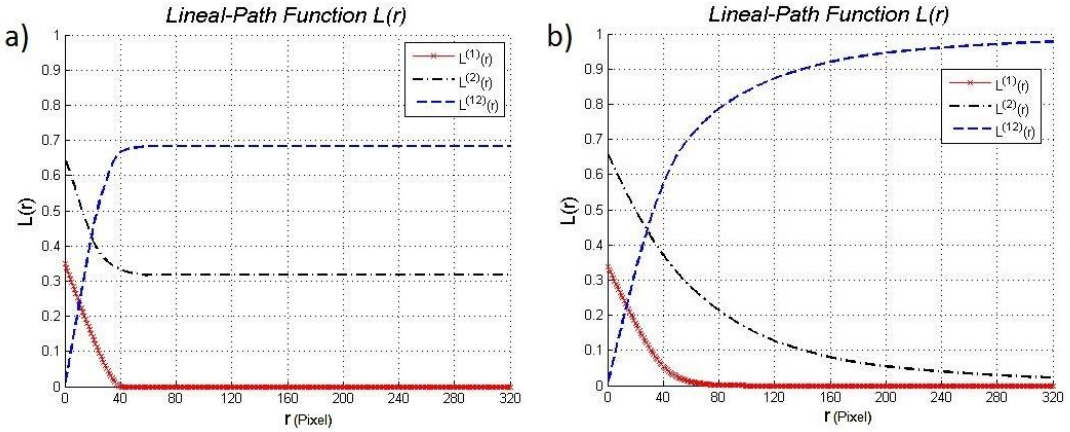

Figure 2.8. (a) Lineal-path functions of long-range ordered microstructure (as shown in Figure 2.5) and (b) without long-range order (as shown in Figure 2.6)

As it can be observed in Figure 2.8the largest length of line section with non-zero probability that can lie in the phase 1 in the long-range ordered microstructure is 40 pixels, and it is equal to the diameter of the circular inclusions in Figure 2.5. Since all the inclusions have exactly the same size and geometry, the lineal-path function for inclusions decreases with sharp slope until it reaches its minimum value of zero. On the other hand, the lineal-path function for inclusions of microstructure in Figure 2.6

decreases very smoothly near its minimum value since the major diameters of the inclusions possess various lengths. The probability of finding a line section with length greater than 80 pixels is very close to zero which means that a few inclusions have major diameters bigger than 80 pixels. Moreover, the largest length of line section with non-zero probability that can lie in the phase 1 is 100 pixels. This number indicates the length of the longest major diameter of all inclusions.

2.2.4. Chord-length Density Function

The chord-length probability density function $p^{(i)}(r)$ [54], also called the chord-length distribution function [55] is a statistical measure defined based on the lineal-path function. In here, chords are all of the line segments located between intersections of an infinitely long line with the two-phase interface. In statistically isotropic microstructures, $p^{(i)}(r)dr$ represents the probability of finding a chord of length between r and $r+dr$ in the phase of interest i, and this probability distribution function normalizes to unity as:

$$\int_0^\infty p^{(i)}(r)dr = 1 \tag{2.25}$$

Then, the mean chord length $l_C^{(i)}$ for the phase of interest i is obtained by:

$$l_C^{(i)} = \int_0^\infty r p^{(i)}(r)dr \tag{2.26}$$

It has been established that the mean chord length value can be written as a function of volume fraction φ_i and the specific surface s for the first three d-dimensional as [56]:

$$l_C^{(i)} = \begin{cases} \dfrac{2\varphi_i}{s}, & d = 1 \\ \dfrac{\pi\varphi_i}{s}, & d = 2 \\ \dfrac{4\varphi_i}{s}, & d = 3 \end{cases} \tag{2.27}$$

Consequently, the chord-length probability density function can be related to the second derivative of lineal-path function by following equation [55]:

$$p^{(i)}(r) = \frac{l_C^{(i)}}{\varphi_i}\frac{d^2L^{(i)}(r)}{dr^2} \tag{2.28}$$

The application of this correlation function can be mainly found in study of gas diffusion and radiative transport in porous media [57-59], and fluid flow through porous materials such as sedimentary rocks [60].

2.2.5. Pore-size Functions

The term of pore-size probability density function $P(r)$ or pore-size distribution function was first applied by Prager [61] for characterization of porous media. However, this distribution function can be applied to any type of three-dimensional microstructured systems. In isotropic microstructures, $P^{(i)}(r)dr$ is defined as probability that a randomly chosen point in phase of interest i lies at a distance between r and $r+dr$ from the nearest point on the interface of two phases. Figure 2.9 demonstrates the schematic event of the pore-size probability density function. This function has its maximum value at origin which equals to interfacial area per unit of phase volume written as: $P^{(i)}(0)=s/\varphi_i$ and it approaches zero at large value of r. Similar to all other probability density functions, this function normalizes to unity as:

$$\int_0^\infty P^{(i)}(r)dr = 1 \tag{2.29}$$

Then, the associated complementary cumulative distribution function is defined as pore-size function $F^{(i)}(\delta)$ with following equation:

$$F^{(i)}(\delta) = \int_\delta^\infty P^{(i)}(r)dr \tag{2.30}$$

Which indicates that the pore-size function is a non-increasing function that approaches zero at very large value of δ, and its maximum value is one at origin. This function is associated with the probability that a sphere of radius r lies entirely in the phase of interest. In other words, it is the three dimensional version of lineal measure and includes the information of connectedness in the phase of interest. Since this function is intrinsically three-dimensional statistical descriptors, it cannot be evaluated from two-dimensional cross-section of media. Correspondingly, the term spherical contact distribution function in stochastic geometry [53] refers to the quantity of $1- F^{(i)}(\delta)$.

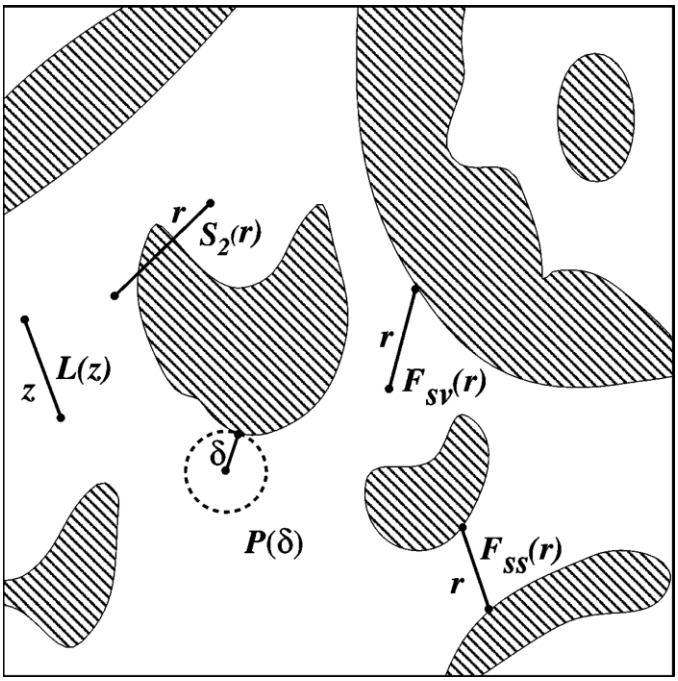

Figure 2.9. A schematic of events that contribute to lower-order functions for two-phase random microstructure. Functions which are shown for white phase include: two-point correlation function $S_2(r)$, two-point surface-surface and surface-void functions $F_{ss}(r)$ and $F_{sv}(r)$, lineal-path function $L(z)$, and the pore-size density function $P(\delta)$ [62].

2.2.6. Cluster Functions

A cluster in a phase *i* is defined as any topologically connected part of the phase that can be reached from a point in the same phase *i* without passing through any other phases. Since clustering in multiphase microstructures has a significant effect on macroscopic mechanical properties, two-point cluster function has been introduced to extract the clustering information[63]. The two-point cluster function $C_2^{(i)}(\vec{x}_1, \vec{x}_2)$ has been defined similar to two-point correlation function but in a connected subset of the whole phase as a probability of finding two point in a cluster of phase of interest. Therefore, it is the only low-order statistical descriptors which contain topological connectivity information of a heterogeneous system. This function can be mathematically defined as:

$$C_2^{(i)}(\vec{x}_1, \vec{x}_2) = \left\langle I_k^{(i)}(\vec{x}_1) I_k^{(i)}(\vec{x}_2) \right\rangle \tag{2.31}$$

Where $I_k^{(i)}(x)$ is defined as:

$$I_k^{(i)}(x) = \begin{cases} 1, & \text{if } \mathbf{x} \in V_i^{(k)}, k \text{ indicates a cluster of phase } i \\ 0, & \text{otherwise} \end{cases} \quad (2.32)$$

Similar to the definition of two-point correlation function in statistical homogeneous media, the two-point cluster function is only related to displacement between the two points $\vec{\boldsymbol{r}}=\vec{\boldsymbol{x}}_2-\vec{\boldsymbol{x}}_1$ as $C_2^{(i)}(\vec{\boldsymbol{r}})$ in statistical homogeneous but anisotropic media. Accordingly, if the homogeneous media are also statistically isotropic then the two-point cluster function is only dependent on the distance $r=|\vec{\boldsymbol{r}}|$ between two points written as $C_2^{(i)}(r)$. Based on the definition, this function also possesses following properties:

$$C_2^{(i)}(0) = \varphi_i \quad (2.33)$$

$$\lim_{r\to\infty} C_2^{(i)}(r) = 0 \quad (2.34)$$

As an illustration, the two point cluster function for inclusions in two-phase isotropic media in presence and absence of long-range order as shown in figures 2.5 and 2.6 are depicted in Figure 2.10.

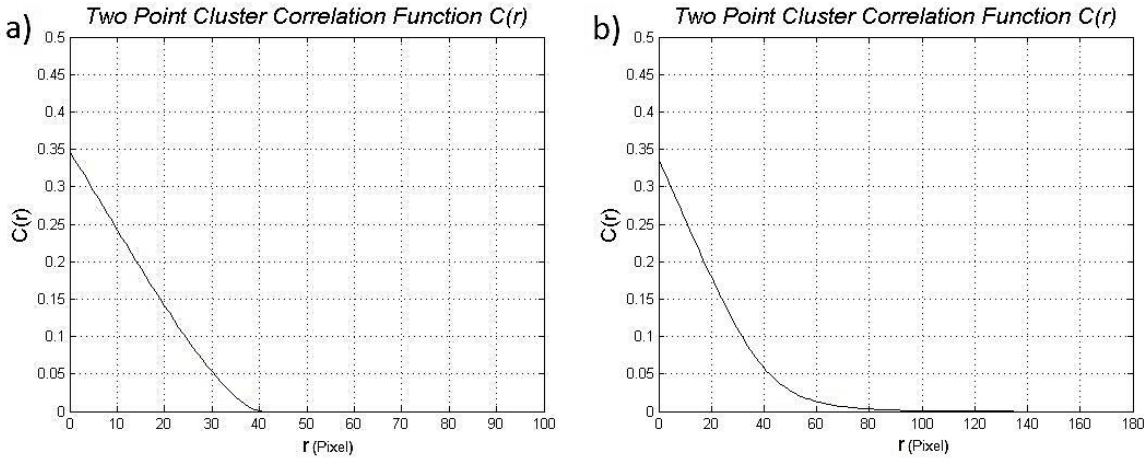

Figure 2.10. Two-point cluster function: (a) long-range ordered microstructure (as shown in Figure 2.5) and (b) without long-range order (as shown in Figure 2.6)

As it can be observed in Figure 2.10, the two-point cluster functions for inclusions in both microstructures are the same as lineal-path functions for the same phase due to convexity of the inclusions. In fact, both two-point cluster and lineal-path functions contain exactly the same morphological information for microstructures with convex clusters. However, in the microstructures that consist of inclusions with concave geometry, the lineal-path functions and two-point cluster function convey different information about the clusters.

2.2.7. Nearest-neighbor Functions

In contrast to all of the aforementioned statistical descriptors which can be applied for any arbitrary type of random media, the nearest-neighbor functions are defined for special case of microstructures consisting of spherical particles distributed randomly throughout another material. In homogeneous media, the particle center nearest-neighbor probability density function $H_P(r)$, also called the nearest-neighbor distribution function, was initially considered by Hertz [64] for characterization of random particles in a material system. Subsequently, it was utilized in characterization of suspended particles in slow viscous flows by Keller et al. [65], random particles in simple liquids by Finney [66], biological systems by McNally and Cox [67], and morphology of amorphous solids by Zallen [68]. In definition, $H_P(r)dr$ indicates the probability that an arbitrary particle center in a system lies at a distance between r and $r+dr$ from the center of the nearest particle [69]. Additionally, another nearest-neighbor function $H_V(r)$ has been introduced in the scaled-particle theory of liquids [70] referred to void nearest-neighbor probability density function. The quantity of $H_V(r)dr$ is defined as the probability that an arbitrary point in a system lies at a distance between r and $r+dr$ from the center of the nearest particle. The complementary cumulative distribution functions of these nearest-neighbor functions are called exclusion probabilities $E_P(\delta)$ and $E_V(\delta)$ and mathematically show as:

$$E_P(\delta) = 1 - \int_0^{\delta} H_P(r)dr \tag{2.35}$$

$$E_V(\delta) = 1 - \int_0^{\delta} H_V(r)dr \tag{2.36}$$

In definition, $E_P(\delta)$ is the probability of finding a spherical region of radius δ centered at some arbitrary particle center empty of other particle centers. Similarly, $E_V(\delta)$ is the probability of finding a spherical region of radius δ centered at some arbitrary point in the system empty of other particle centers. Assuming identical spheres with radius R randomly distributed in a system, $E_V(\delta)$ indicates the fraction of space which is available to insert a sphere of radius δ-R into the system. These probability functions have been studied by Vezzetti [71], Ziff [72] , and Truskett et al [73] among other researchers in the field of statistical mechanics.

Correspondingly, some other nearest-neighbor functions, also called nearest-surface functions, have been introduced by Lu and Torquato [74] which are defined based on the surface of the nearest particle instead of its center and denoted as $h_P(r)$, $h_V(r)$, $e_P(\delta)$, and $e_V(\delta)$. For example, $h_P(r)dr$ is defined as the probability that an arbitrary particle center in a system lies at a distance between r and $r+dr$ from the nearest particle surface, and $h_V(r)dr$ is defined as the probability that an arbitrary point in a system lies at a distance between r and $r+dr$ from the nearest particle surface. Both $e_P(\delta)$ and $e_V(\delta)$ are the complementary cumulative distribution functions for $h_P(r)$ and $h_V(r)$ respectively, and can be mathematically defined in the same way of Equations (2.35) and (2.36). In a system containing identical spheres R in which the particle surface information is directly dependent on center particle information, following equations are valid:

$$h_P(r) = H_P(r+R) \tag{2.37}$$

$$h_V(r) = H_V(r+R) \tag{2.38}$$

$$e_P(\delta) = E_P(\delta + R) \tag{2.39}$$

$$e_V(\delta) = E_V(\delta + R) \tag{2.40}$$

However, in a system with spheres in various sizes, the surface quantities contains different information than the center quantities, because the sphere with the nearest center my not be the same as the sphere with the nearest surface. It should be also noticed that

in inhomogeneous systems, all the aforementioned quantities are functions of the vector $\vec{r}$ instead of absolute value of the distance.

2.2.8. Computation of Statistical Functions

Many efforts have been made to represent the statistical function in analytical forms. Most of these analytical formulas can just give an approximation for some of the statistical functions in specific microstructures with spherical inclusion. The analytical formulas of n-point correlation function, surface correlation function, lineal-path function, and chord-length function for different types of spherical inclusions can be found in the literature [49, 52, 55, 75-82]. Some other formulas have been also proposed to fit the decreasing trend of two-point correlation in general type of microstructures. Most of the fitting functions that can be found in literature [83-86] use exponential function with some fitting parameters which do not convey any physical meaning, and do not represent the fluctuations observed in the long tail of the true correlation functions (as it is shown in Figure 2.5 and Figure 2.6). These fluctuations are important because they contain nontrivial information of dispersion status of the microstructure, such as the nearest distances between clusters [87]. Additionally, one hybrid exponential-sin function has been also developed to capture the fluctuation feature [88], but this function also use fitting parameters which must be determined based on the morphological class of microstructure and do not have any physical meaning. In the latest attempt, Xu et al [89] proposed an analytical form of two-point correlation function for low volume fraction, less than 15%, nanoparticle-reinforced polymer composites' microstructure using average value of physical parameters such as volume fraction, radius of particles, nearest center distance, and elongation ratio of the particles. However, this formula cannot accurately represent the fluctuations, and fail to represent the dispersion status of inclusions. To sum up, none of the proposed analytical formulation of correlation functions up to now could convey all of its information. Therefore, computational methods are used in practice to obtain different correlation functions.

2.2.8.1. Monte Carlo Method

In computing, a Monte Carlo algorithm is based on random sampling to obtain numerical results with a certain probability. For example, in a Monte Carlo algorithm for computation of two-point probability function of a sample microstructure, two points with specific distance are randomly selected several times and the number of times both points lie in the same phase of interest is divided by the total number of random selections of two points. The accuracy of the results in this algorithm can be improved by increasing the number of random selections. Figure 2.11 demonstrates the value of two point probability function of inclusions for r = 10 with respect to the number of coupled points with relative distance 10 pixels that are selected in the sample image shown in Figure 2.6 with size of 1200 by 1200 pixels. As it can be observed this method gives good approximation of two-point correlation function after about 6000 iteration which is reasonable number of iteration for an image with 1.44E6 pixels.

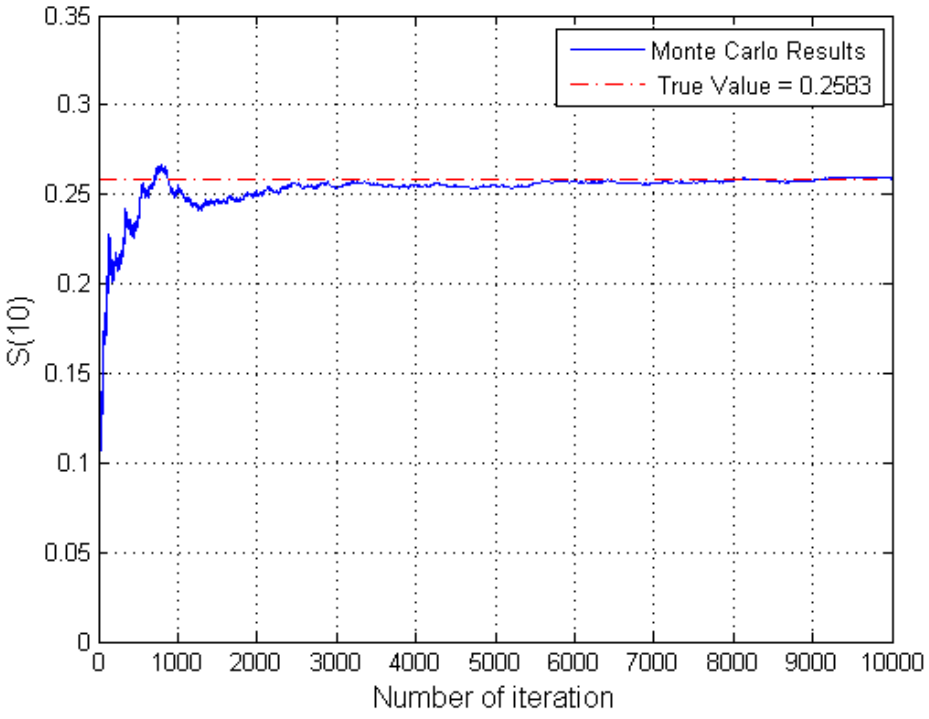

Figure 2.11.Two point correlation function using the Monte Carlo simulation for length of 10 pixels

This algorithm can also be used for obtaining other correlation functions such as lineal-path function by randomly selecting a line with specific length in the image and counting the number of times that the line lies entirely in the phase of interest. Dividing this number by the total number of line selection will give the lineal-path probability function for the phase of interest. Although this algorithm does not provide a deterministic result for statistical correlation functions, but it can give a good approximation for large images with a reasonable computational cost.

2.2.8.2. Counting Method

In contrast to Monte Carlo algorithms, the counting algorithms are based on considering all the points or pixels in a digital image to obtain the correlation functions. Therefore, the results are deterministic for that sample image which has been chosen for characterization. However, the counting algorithms are usually computationally expensive. For example, to obtain two-point correlation function from a digital image, all the value of the pixels must be checked and the distance between all the pixels in the image must be also measured. For this counting problem, two different algorithms have been proposed.

The primary algorithm initiates with checking the first pixel at the first row and column of image and the points located on the circles which are centered at the initial point. Since the initial point is selected at top-left of the image, a quarter circle with growing radius can cover all the other pixels in the image. All the pixels located on the circle with radius r and the same phase as the initial point are stored as the couple for the initial point specified with the distance r. After checking all the pixels for the first point, the algorithm goes to the point at the next column and checks all the possible couple for that point. When it reaches the point at the last column, the next point will be the point at the second row and the first column. In this algorithm, depending on the position of the point, just a section of the circle must be checked. For instance, for all the points located at the left border of the image a quarter of the circle is enough to cover all the points that

can be selected as their couples. Since the points that have been already selected as a center of the circles will not checked again, the maximum section of the circle which should be consider for point searching is a half circle because the points of the other half have been already selected as the center of searching circle and counted as the possible couple for that point. This algorithm can store all the possible two-point correlation functions for the microstructure simultaneously. Although this algorithm avoids any repetition of counting, it does not use any information of pixels' values to reduce the computational cost. Thus, a different algorithm has been also proposed.

In the second algorithm, the positions of the pixels in each phase are stored in different places. Then, the distances between all the points that belong to the phase of interest are calculated. The number of distances with length r is divided by the total number of line section with length r that can lie entirely in the image. The advantage of this algorithm comparing to the first one is that calculating two-point correlation function of each phase can be done independently. Since as it is mentioned before, just one out of four two-point correlation functions for a two-phase material is independent, this algorithm can reduce the computational time by avoiding extraction of extra information. The result of this algorithm is verified by two-point correlation function plot published in [89]. Moreover, similar algorithm can be also modified and utilized for calculating three-point correlation function. However, the computational cost for three-point correlation function is very high and it can just be calculated for a small sample image in a reasonable amount of time.

The two point cluster function can be also calculated in the same way of two-point probability function. However, the clusters in the image must be labeled before utilizing the counting algorithm. In this way, the information of each cluster can be obtained separately. Since the clusters of a phase are smaller subset of the phase, the computation cost for the two point cluster function is less than two point correlation function.

Another algorithm is proposed for lineal-path function. This algorithm reads the binary image and allocates an array *L(i,r)* to store the number of horizontal lines with length *r* that lie in the phase *i*, where *r* is measured in pixels (e.g. *r = 1* indicates a line with one pixel length which is the same as one point in the image). The code starts by scanning the image line by line. The value of each pixel is checked starting from the first pixel in the horizontal line. The code keeps on moving to the next pixel until the phase changes. This gives the number of pixels in row in that particular phase, let say *i*. At this time, the values of the arrays *L(i,r)* are increased by one in which the line segment was observed. For example, if 10 pixels of phase 1 are encountered, the value of *L(1,1)* is increase by 10, *L(1,2)* by 9 (since nine line segments with length of 2 pixels can be landed on a line of 10 pixels) and so on. The code then continues along the same line till another phase change or end of line is reached. This gives the *L(i,r)* values for a single line and the procedure is repeated for all the horizontal lines in the image to get the total number of *L(i,r)* in the x-direction. The total number of possible line segments (for each *r*) in the image with *nelx* pixels in x-direction and *nely* pixels in y-direction is calculated using this formula: $nely \times (nelx - r + 1)$. Then, the lineal path probability function for the given direction is calculated by dividing the number of lines found with length *r* in the phase of interest by the total number of length segments possible in the image for that length. Similar procedure can be used to compute the lineal paths along other directions as well.

Other aforementioned statistical function can be also calculated using similar algorithms, but this study focuses on calculating two and three point correlation functions, two point cluster function, and lineal-path function for microstructure characterization. It will be shown in next chapter that these functions give enough information for reconstruction of some sample microstructures.

2.3. Physical Descriptor-based Characterization

Another approach for characterization is based on physical parameters of morphological features of different phases in a material system. Area of each phase and its clusters is one of the basic physical parameters that can be easily obtained. As mentioned before, this physical parameter can be also obtained by one point correlation function and cluster function for the entire phase or its clusters respectively. The perimeter of each cluster can be also calculated by function coded in MATLAB. This value is equal to the one point surface correlation function, so it can be also found directly with a statistical correlation function as well. This parameter is basically important when the interface of phases has significant influence on the desired mechanical property. For example, in optimization problem of electrical or thermal connectivity this parameter plays an important role and as an optimization variable. Moreover, the roundness of each cluster can be found using its area and perimeter by following equation:

$$Roundness = \frac{4\pi \times Area}{(Perimeter)^2} \tag{2.41}$$

If the Roundness is greater than 0.90 then, the cluster is circular in shape. Correspondingly, the diameter of a circle with the same area can be computed as $\sqrt{4Area/\pi}$. The other physical parameter that can be obtained using a MATLAB function is the location of the centroids of the clusters in a material system. This parameter is mainly useful for describing the distribution of fiber or grains in composite matrix.

In addition, some physical parameters can be defined based on modeling each cluster with an ellipse that has the same normalized second central moments. After modeling each cluster as an ellipse shape, following parameters can be defined and calculated: Major and minor axes length of the equivalent ellipse. The eccentricity of the equivalent ellipse is the ratio of the distance between the foci of the ellipse and its major axis length. The orientation of the cluster is the angle in degrees ranging from -90 to 90 degrees between the x-axis and the major axis of the equivalent ellipse. These parameters

are very useful for modeling the random shape of inclusions for example grains in composite ceramics. However in such a rough modeling the effect of curvatures in the random morphology of inclusions will be ignored. These physical properties for a small sample consisting of six clusters as shown in Figure 2.12 are presented in Table 2.1.

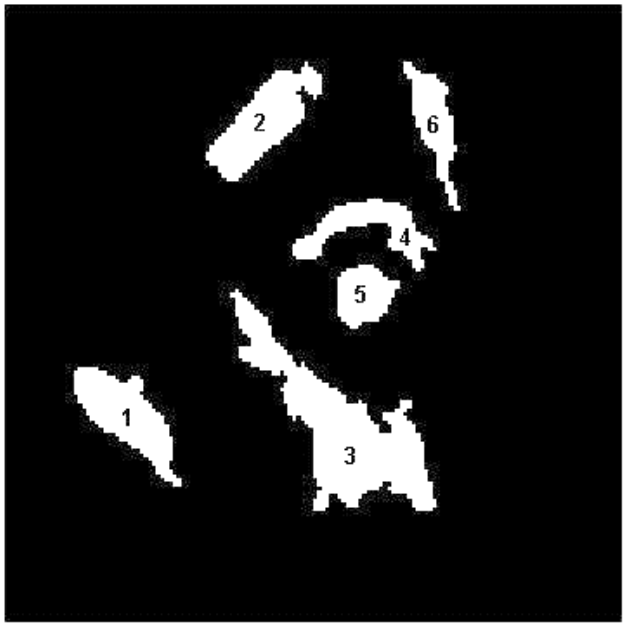

Figure 2.12. A sample media consists of six random shaped clusters

Table 2.1. Physical properties of clusters in Figure 2.12

Cluster Number	1	2	3	4	5	6
Area (Pixels)	332	350	852	235	168	199
Perimeter	90.57	92.71	218.69	103.74	48.04	86.18
Roundness	0.71	0.72	0.47	0.52	0.96	0.58
Equivalent Circular Diameter	20.56	21.11	32.94	17.30	14.63	15.92
Major Axis Length	34.76	36.26	66.56	37.82	15.84	34.47
Minor Axis Length	13.37	12.91	23.88	16.48	13.92	8.70
Eccentricity	0.9231	.9344	.9334	0.9000	0.4773	0.9676
Orientation (Degree)	-45.42	46.9	-45.40	0.21	54.81	-74.98

However, the physical descriptors are not limited to aforementioned parameters. In fact, depending on a geometry and shape of a cluster, one can define many other physical parameters. For example, some simple geometry like circle or ellipse can be characterize just by a few parameters which have been mentioned here, but a completely random shape like cluster number 3 my need much more number of parameters to be characterized with reasonable amount of accuracy. In Figure 2.13.b-f, the histograms of some physical parameters of sample optical microstructures of magnesium alloy (shown in Figure 2.13.a) are demonstrated.

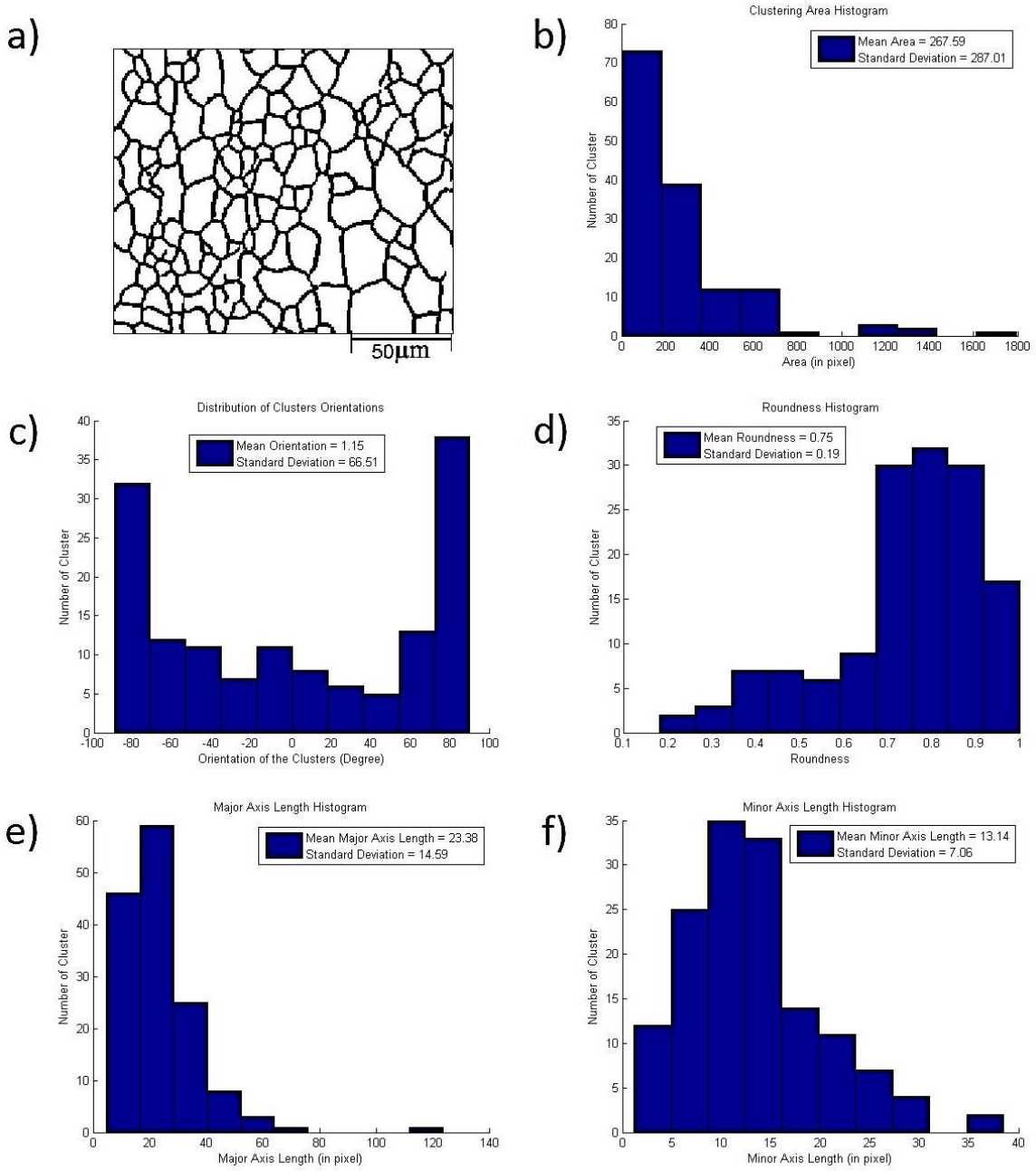

Figure 2.13. Histograms of physical properties of clusters in sample (a) magnesium alloy: (b) area, (c) orientation, (d) roundness, (e) major axis, and (f) minor axis.

2.4. Comparison of Statistical and Physical-based Characterization

Statistical and physical characterizations are fundamentally based on completely different concepts. Statistical functions are based on probabilities of some events which are related to the morphological features. On the other hand, physical parameters are based on measuring these features. Therefore, each physical parameter directly indicates a morphological feature in contrast to the general statistical functions which contain combination of many of these features without explicitly conveying them. For instance, it has been shown in literatures [82-86, 88] that two-point correlation function can be written as some morphological parameters for specific type of heterogeneous materials, but in general, the physical parameters cannot be extracted directly from the general statistical correlation functions. However, since the statistical descriptors contain more complex features of random shapes, they can be used for reconstruction of a model which contains more detailed features of the actual microstructure. Contrarily, although physical descriptors can give an accurate reconstructed model for simple regular shape of inclusions such as disk or ellipse, but they give rough approximation of a random shape unless all the physical features of the shape can be extracted and used in the reconstruction, which is not feasible for many cases. Moreover, a random microstructure usually includes many different random shapes of the clusters with random distribution. Thus, the number of physical parameters which are needed for complete characterization of entire random heterogeneous microstructure approaches infinity. Nevertheless, the mean value of some important physical parameters can still be utilized to construct a model which possesses the average morphological features of the microstructure. In next chapter, it will be presented how these characterization approaches can be utilized for reconstruction of microstructures.

3. MATERIAL RECONSTRUCTION

The main purpose of material reconstruction is to model a microstructure using the characterization parameters which possess the same mechanical behavior. The accuracy of the reconstructed model depends on the characterization parameters that are utilized in the reconstruction process. In general, infinite characterization parameters are needed to describe arbitrarily highly random media. However, most of the microstructures are generated based on some rules such as processing rules in synthesis materials or biological rules in bio-materials, which implement some limitations in morphological patterns which in fact reduce the randomness in these microstructures. Therefore, finite number of characterization parameters can be utilized in many cases for reconstruction. A successful reconstruction, which possesses the same mechanical properties of actual microstructure, verifies the sufficiency of the characterization parameters for describing the morphological features of the microstructure. In this chapter, first the traditional statistical reconstruction is introduced and the limitations of this approach are discussed. In the next section of this chapter, cellular automaton (CA) as a reconstruction method based on grain growth rules is presented. Then, the CA approach is improved by implementing more physical parameters in its algorithm. However, it is shown that even modified CA method cannot still provide a fully representative mode of the microstructure. In the last section, a new algorithm for reconstruction specific case of microstructures with elliptical inclusions is introduced which is capable of microstructure reconstruction based on its physical parameters.

3.1. Statistical Reconstruction

The statistical reconstruction is the process of recovering a statistically equivalent microstructure using statistical correlation functions. After the characterization of the original microstructure using the statistical descriptors, the reconstruction can be obtained by solving an inverse problem. This problem can be formulated as an optimization problem in which the objective is minimizing the error between statistical descriptors of original image and the reconstructed image [16, 18, 42]. It has been shown that just one single lower-order correlation function such as two-point correlation function cannot provide sufficient information for reconstruction [82]. Therefore, hybrid reconstruction consisting of an arbitrary number of statistical functions can be used to overcome the limitations of individual correlation functions. For example, reconstruction of a two-phase microstructure using two-point cluster function and three-point correlation function can be formulated as following optimization problem:

Minimizing:

$$E = \sum_{r=0}^{Rmax} (C_2^{(i)}(r) - \hat{C}_2^{(i)}(r))^2 + \sum_{\mathbf{r}_{12}=0}^{Rmax} \sum_{r_{13}=0}^{Rmax} (S_3^{(i)}(r_{12}, r_{13}) - \hat{S}_3^{(i)}(r_{12}, r_{13}))^2 \quad (3.1)$$

Where $\hat{C}_2^{(i)}(r)$ and $\hat{S}_3^{(i)}(\mathbf{r}_{12}, \mathbf{r}_{13})$ are the correlation functions of the digitized medium at each of the discrete distance values r, and $C_2^{(i)}(r)$ and $S_3^{(i)}(\mathbf{r}_{12}, \mathbf{r}_{13})$ are correlation functions for original (target) microstructure. E is norm-2 error or fictitious energy at any particular stage. R_{max} is the integer magnitude of the longest vector that can lie on the image. This problem cannot be easily solved by traditional gradient based optimization algorithms due to its complexity and high nonlinearity. Hence, some stochastic methods such as simulated annealing [82, 90, 91] and genetic algorithms [92] have been employed to find the optimal solution of this problem. In this study, the simulated annealing algorithm is used to solve the reconstruction problem. After generation of an initial binary medium with both phases having the same volume fraction as the original microstructure, a new model is created by interchanging the states of two selected pixels

of different phases to preserve the volume fraction of each phase. Then, the change of the error $\Delta E = E_{new} - E_{old}$ between the two successive models is calculated. The new model is accepted with some probability $p(\Delta E)$ which is related to the error change. This probability function is defined as:

$$p(\Delta E) = \begin{cases} 1 & \Delta E \leq 0 \\ exp(-\Delta E/T) & \Delta E > 0 \end{cases} \quad (3.2)$$

Where T is a fictitious temperature chosen initially so that the first acceptance probability for interchange two pixels with $\Delta E > 0$ averages approximately 0.5. The temperature will decrease in each iteration with a coefficient less than one but very close to it. The iterative process will terminate when the error is lower than a small value, e.g. ε = 1.0E-4 or the unsuccessful iteration gets higher than a very large number e.g. it_{max} = 1.0E6. The schematic of this algorithm is shown in Figure 3.1.

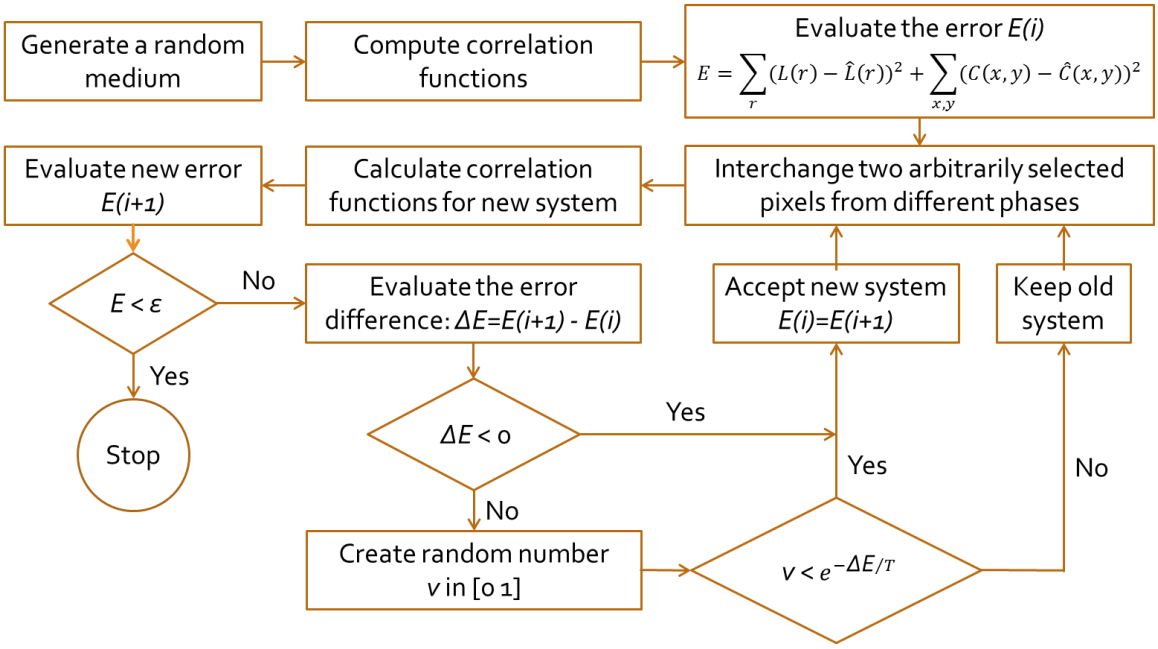

Figure 3.1. Statistical reconstruction algorithm

A sample of statistical reconstruction process using this algorithm is shown in Figure 3.2.

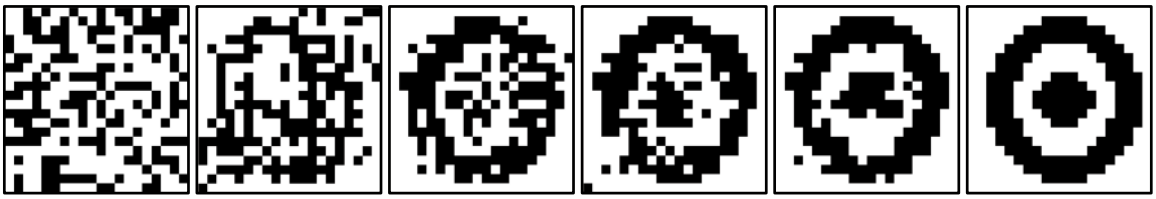

Figure 3.2. Statistical reconstruction process: Left: initial random material distribution. Right: achieved target design

Although this method can be successfully used for reconstruction of any arbitrary microstructure but the disadvantage of using this reconstruction approach is its high computational cost which limits its usage to reconstruction of small samples. The expensive computational cost is due to selection of a random point in each iteration and evaluation of all the correlation function for each new model. Moreover, since there is no condition for selecting the random points to interchange, the algorithm freezes at high number of iterations, and when just few points are left to decrease the error, the algorithm spend lots of time to find those few points. Another factor in this algorithm that causes its expensive computational cost is its start point of search which is an arbitrary media created randomly. To overcome the aforementioned problem with this traditional reconstruction method, a new method is proposed in Section 3.4 which can improve the computation cost of this algorithm by changing the trend of choosing random points in interchange process and adjust the starting media by means of some physical conditions.

3.2. Physical-Based Reconstruction in Cellular Automata Framework

3.2.1. Cellular Automata Basics

Cellular automata (CA) framework of microstructure simulation was first proposed by von Neumann[93] and employed in scientific field by Wolfram [94] Since then this method has been broadly used by scientists and researches[95-98] as an effective tool to reproduce the process of microstructural evolution in metal forming such as recrystallization and recovery [99-101] related nucleation and coarsening phenomena

[102-105], as well as formation of dendritic grain structures in solidification processes[102].

The CA method utilized physically based rules and provides a simpler physical realization of folding on a regular lattice in two and three-dimensional spaces. This model is computationally more efficient than statistical reconstruction and it can be easily incorporated in a fixed-mesh finite element analysis framework. The two-phase microstructural simulation model incorporated in this study has two stages for inclusion phase: nucleation and growth. Nucleation sites are randomly assigned preserving a critical box distance. The maximum number of nucleation sites is unknown a priori and should be determined by simulation as shown in Figure 3.3.

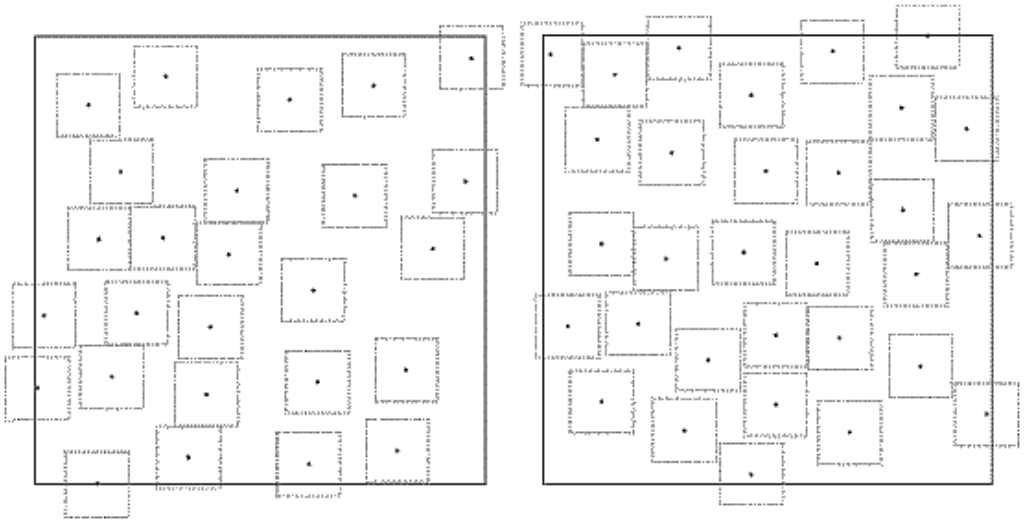

Figure 3.3. Maximum number of nucleation sites obtained in two simulations from the lattice model: 26 sites (left) and 31 sites (right) for a squared periodic domain of size $L \times L$ and critical box distance $0.14L$.

The growth is defined by recrystallization kinetics of the parent phase surrounding the nucleation sites. The CA method incorporated determines the transformation of the parent phase in the neighborhood of a grain without regard of the energy field intruded by the grain, i.e., a neighboring parent phase is transformed with a given probability. The grain growth is therefore a function of both the neighborhood size

and probability of transformation. The neighborhood N_i of a cell i in a CA lattice is defined by:

$$N_i = \{j: d(i,j) \leq r\} \tag{3.3}$$

Where $d(i,j)$ is the distance between cells i and j, and r is the size of the neighborhood. If all neighboring parent-phase cells are transformed, the topology of the grain is determined by the size of the neighborhood as shown in Figure 3.4.

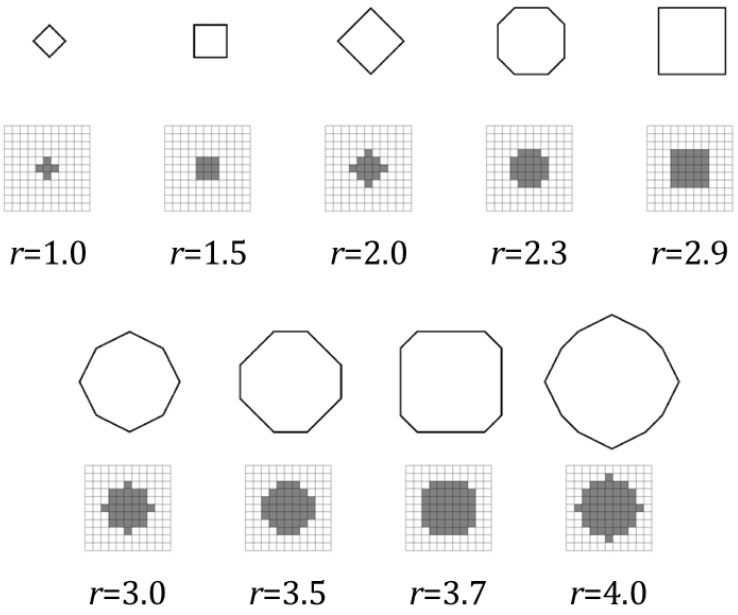

Figure 3.4. Grain topology as function of the CA neighborhood after a constant number of time steps. In each time step, all neighboring parent-phase cells are transformed.

If the transformation occurs with a given probability p, such probability also determines the topology of the grain as shown in Figure 3.5.

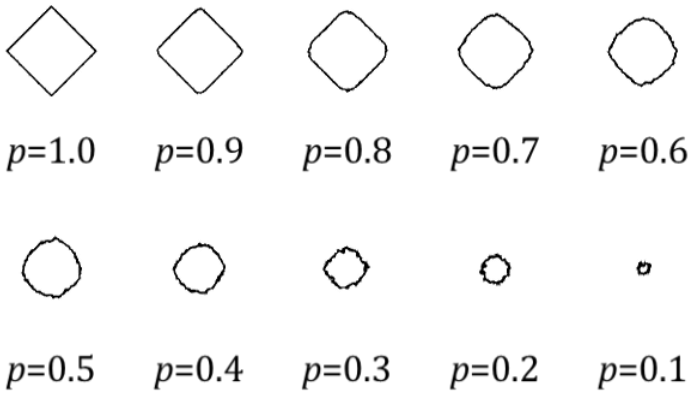

Figure 3.5. Grain topology as function of the probability p of transformation after a constant number of time step for a neighborhood size r = 1.0.

Bias grain growth can be also incorporated by modifying the neighborhood layout. A comparison of models with and without bias is shown in Figure 3.6.

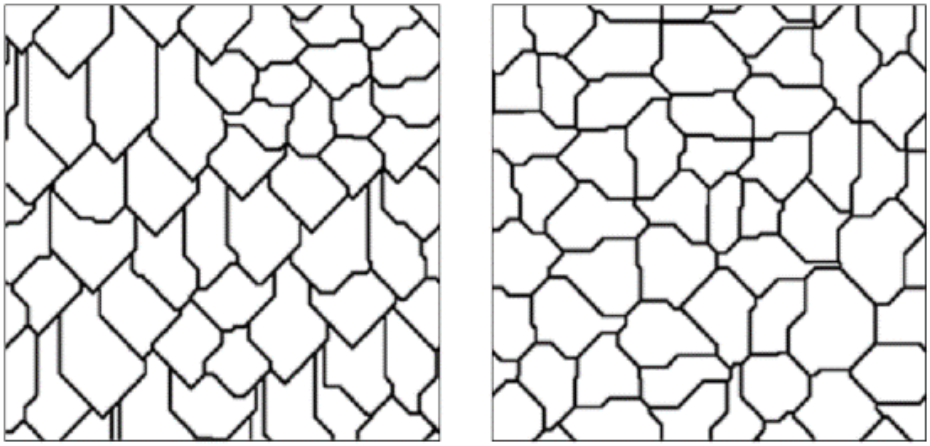

Figure 3.6. Microstructural for 40 grains, r = 1.0 and p = 1.0 with bias (left) and without bias (right).

Although this method can simulate the evolution of crystalline microstructures much faster than statistical reconstruction approach, but the resulted CA model lacks the statistical equivalency of the actual microstructure in most cases. Since the rules employed for all the inclusions are the same, the average size and shape of the modeled inclusions are very similar with uniform distribution of physical parameters. The schematic of grain growth process in CA simulation is shown in Figure 3.7 from (a) to

(e). The objective of this modeling is to reach a microstructure shown in Figure 3.7.f, but as it can be seen, many differences between distributions of sizes and locations of the grains in two microstructures are available. In order to implement these features in CA simulation, the modification of this algorithm is proposed in the following section.

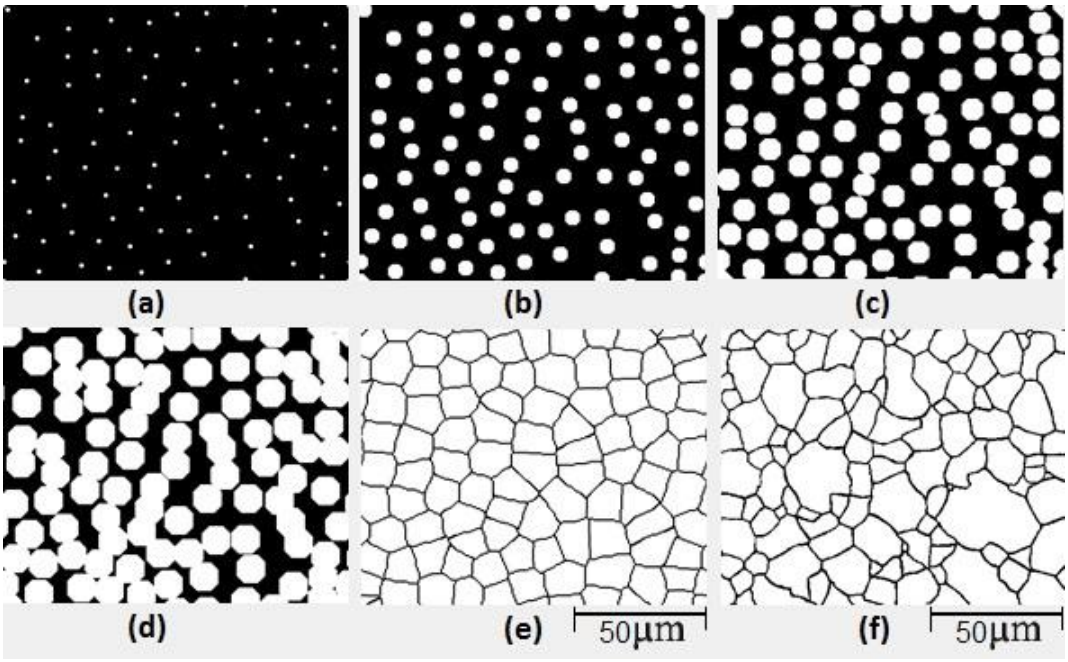

Figure 3.7. (a-e) Growth steps of CA modeling and (f) target microstructure

3.2.2. Modified Algorithm of Cellular Automata

It has been shown that the basic algorithm of CA which based on random distribution of nucleation sites can just give a rough approximated model of the microstructure and it lacks provide the grains distribution of the actual medium. Therefore, the basic algorithm is modified to employ more physical features in its simulation. For example, in the modified algorithm the relative distances between grains' centroids are evaluated and the nucleation sites are located according to theses distances from each other. This additional rule in the CA let nucleons have distribution similar to actual microstructure. Since the grains grow according to the space allocated by grains in its neighborhood, the variety size of growth can occur in this modified algorithm which

depends on the state of neighborhood. The model resulted from the modified CA algorithm is shown in Figure 3.8.c comparing to simple CA model shown in Figure 3.8.b. In order to show the improvement of the modified CA model with respect to the basic CA model the two-point correlation functions for these models and the actual microstructure are depicted in plot (Figure 3.8). As it can be observed the correlation between modified CA is much higher than the CA model due to more similarity between sizes and position distribution of the grains. However, the fluctuations of the two-point correlation function for modified CA model still follows different pattern than the actual microstructure which is due to differences between configuration shown in Figure 3.8.a and Figure 3.8.b. As it can be observed the two point correlation functions for Modified CA and the target microstructure match very well when r is less than 15 pixels, which indicates that two microstructures possess equal volume fraction and each point in both media have similar short range neighborhood. However, the considerable errors between tow functions when r is in the range of 15 to 180 pixels are caused by the absence the grain size variations of target microstructure in the modified CA model. Moreover, the two point correlation function of modified CA shows diverging behavior with respect to the actual model's correlation function which indicates the decrease of correlation between two microstructures in long range order.

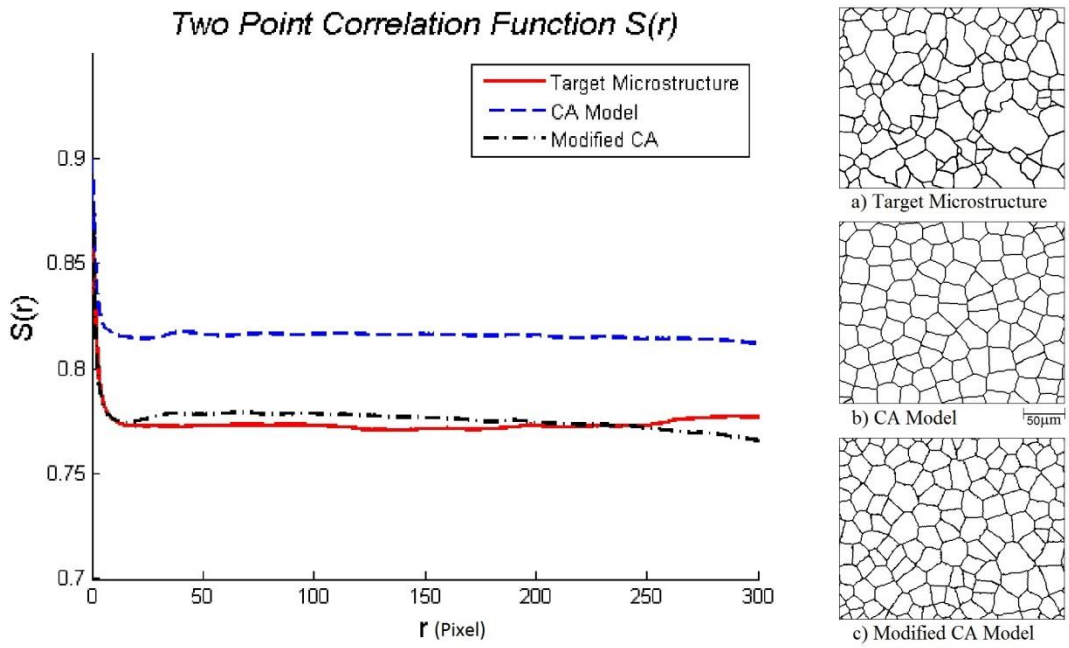

Figure 3.8. Error between two-point correlation function of target microstructure, CA model, and modified CA model

3.3. Physical-Based Reconstruction of Material with Elliptical Inclusions

In this approach microstructured materials can be reconstructed as a model with elliptical inclusions based on physical features of clusters [106]. This type of reconstruction can be unutilized specifically to porous materials, model fiber reinforced composites, and some biological materials such as dentine. The reconstruction algorithm used in this study receives the input parameters such as volume fraction of the inclusions, the average lengths (in pixels) of major and minor axes of the inclusions, and their size and orientation distribution, to generate a model based on this parameters. First, the average size of the inclusions in pixels are calculated for the input aspect ratio of their axes and based on the size of each inclusion and the input volume fraction, the number of inclusions in the medium is calculated. Then the positions of inclusions' centroids are randomly selected and the inclusions are generated based on the predetermined size and orientation distribution parameters. If the one inclusion overlaps the others, the coordinates of its centroid will be changed until it does not have any overlap with other inclusions. Since this algorithm is written to model statistical homogeneous media, the

influence of boundary effects on inclusion placement is mitigated by imposing periodic boundary conditions on the vertical and horizontal edges of the sample domain. Inclusions that extend beyond the sample bounds are wrapped back onto the opposite side of the image.

In this approach two options are available for size distribution of inclusion: the uniform distribution and the log-normal distribution. The lognormal distribution is the maximum entropy probability distribution for a random variable x for which the mean and variance of $Ln(x)$ are fixed. Since in many natural processes of growth, growth rate is independent of size, the log-normal distribution is important in the description of natural phenomena[107]. According to the principle of maximum entropy, if nothing is known about a distribution except that it belongs to a certain class, then the distribution with the largest entropy should be chosen as the default. The motivation is twofold: first, maximizing entropy minimizes the amount of prior information built into the distribution; second, many physical systems tend to move towards maximal entropy configurations over time [108]. In this algorithm for size log normal distribution, the mean value, standard deviation, and the increments can be defined as input. Then, the sizes of clusters are evaluated based on this distribution and assigned to the inclusions.

There are also three possible options for orientation of the inclusions. They can be either oriented all aligned, random, or with normal distribution. If the normal distribution of orientation is selected then the mean, standard deviation, and increments should be entered as input parameters. The reconstructed sample models of elliptical inclusions for different input parameters are shown in Figure 3.9.

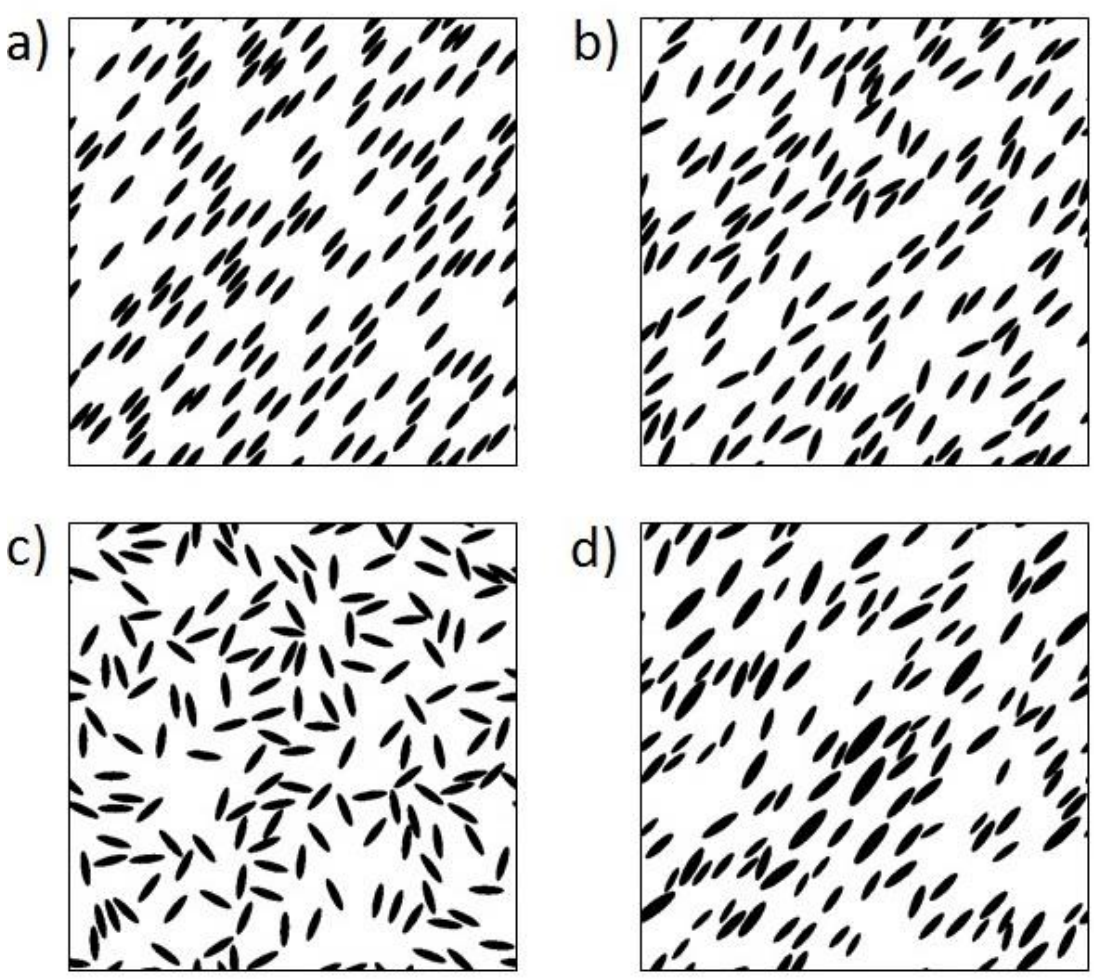

Figure 3.9. (a) Aligned identical inclusions, (b) identical inclusions with normal orientation distribution, (c) identical inclusions with random distribution, and (d) log normal size distribution with normal orientation distribution

4. MATERIALS DESIGN

4.1. Problem Statement

The problem of material design or design optimization can be generally stated as:

$$\begin{aligned} &\text{Find} && \boldsymbol{x} = (x_1, x_2, \ldots, x_n) \\ &\text{Maximize} && \boldsymbol{P} = (P_1, P_{2,\ldots,} P_m) \\ &\text{Subjected to} && \text{Manufacturing Constrains} \end{aligned} \tag{4.1}$$

Where $\boldsymbol{x}$ is a set of morphological characteristic parameters, $\boldsymbol{P}$ is a set of performance functions, and the manufacture constrains are dependent on the type of manufacturing process that can be utilized for each specific material. These parameters all will be defined based on the design problem. The number of morphological parameters that can be selected as the optimization variables is in practice limited to those parameters that can be controlled in manufacturing processes. In this study, one performance of the material is considered as the objective function and the effect of different morphological descriptors is studied based on the type of the microstructure (refer to Section 4.4). Since crack propagation has significant effect on performance of mechanical components, fracture energy is considered as the objective function for both numerical examples. The manufacturing constrains are also applied in modeling procedure of the material.

4.2. Finite Element Analysis

Finite element method (FEM) is utilized to evaluate the performance of materials with different morphological parameters. In this study a simplified model of a two dimensional sample with shell elements is developed based on the digitalized images obtained in MATLAB software and imported to LS-DYNA for finite element analysis. Fixed quadrilateral mesh is created using a one to one pixel to element correspondence in

LS-DYNA. The nodes on the surface of two phases are tied and stick together in order to integrate the whole material. The material properties in room temperature are assigned for each phase. The material parameters for different phases used in numerical examples of Section 4.2 are shown in Table 4.1.

Table 4.1. Material parameters of FE model in numerical examples

Material	Elastic modulus (GPa)	Poisson's ratio	Yield stress (MPa)	Plastic strain
Homogenized magnesium alloy **[109]**	45	0.35	188	0.01
Grain Boundaries **[109]**	45	0.35	150	0.008
Silicon carbide **[110]**	450	0.2	14E3	0.02

In order to model the dynamic of crack propagation, an initial vertical crack from bottom edge of the sample is modeled by eliminating elements corresponding to the size of the crack which has length of one third of the sample. The schematic of finite element model is shown in Figure 4.1. Then, the uniaxial tensile load is applied on the side boundaries to simulate the opening mode (Mode I) of crack propagation. After total failure of sample by rupturing, the fracture energy is evaluated.

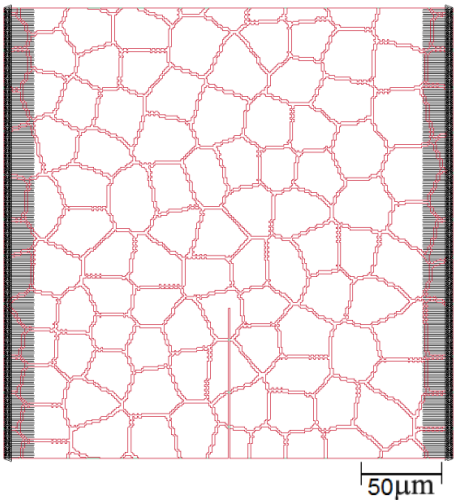

Figure 4.1. Schematic of finite element model with tensile loading boundary condition

4.3. Meta-modeling

Since the variables of material design problem contain infinitive continuum domains, it is impossible to model the entire domain. Moreover, the expensive computational cost of finite element method imposes limitation on analysis of huge sample of variables. Therefore, meta-modeling techniques are utilized to obtain the sensitivity of the performance function to morphological variables. In this investigation, a well-established meta-modeling approach of Kriging [111] is utilized to create surrogate models for sample problems.

Kriging is an optimal interpolation method to predict the value of a function at a given point by computing a weighted average of the known values of the function in the neighborhood of the point. This method is based on regression against observed values of surrounding data points, weighted according to spatial covariance values, and offers the best linear unbiased prediction of the intermediate values. More details and formulations of this method can be found in literatures [111, 112]. In this study a free available software of MATLAB Kriging toolbox [113] is utilized to construct an approximation surrogate model based on results obtained from finite element analyses.

4.4. Numerical Examples

4.4.1. Material with Random Shaped Clusters

Metallic alloys are heterogeneous microstructed materials made of random shaped grains which are widely used in engineering. Magnesium alloys have been of recent interest of many engineers due to high demand of light-weight materials in industry. The AZ31 Mg alloy possess many attractive mechanical properties, including high specific strength, good tensile properties [1] high machinability, and fatigue resistance [114]. Since AZ31 Mg alloy is not as tough as other widely-used Al alloys, lots of efforts have been devoted to studying and improving its fracture resistance. Somekawa and Mukai

[115] have shown that the fracture toughness of AZ31 Mg Alloy can be improved by refining grain structure in an equal-channel angular extrusion process.

In this study an example of design optimization problem for maximization of fracture strength is solved based on morphological variables such as average grain size and average grain aspect ratio. These morphological parameters are selected as optimization variables because they can be controlled by manufacturing process. For example, hot rolling can significantly decrease the size of the grains [116].

To approximate the fracture strength as a function of average grain size and aspect ratio, 50 samples are modeled in CA framework for finite element analysis. Then, the fracture strength value for each sample is obtained by modeling crack propagation through the material as shown in Figure 4.2 for coarse-grained microstructure (a) and fined-grained microstructure (b).

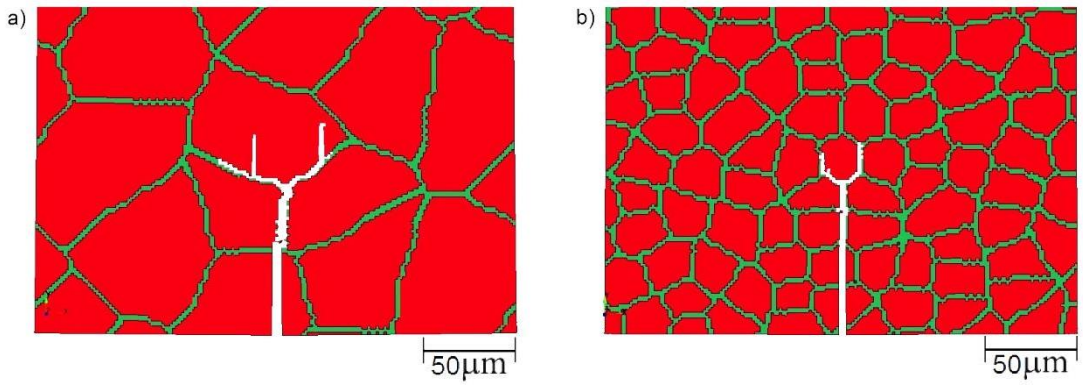

Figure 4.2. The schematic of crack propagation in two samples (a) coarse-grained (b) fined-grained

The Kriging surrogate model obtained through samples is illustrated in Figure 4.3.

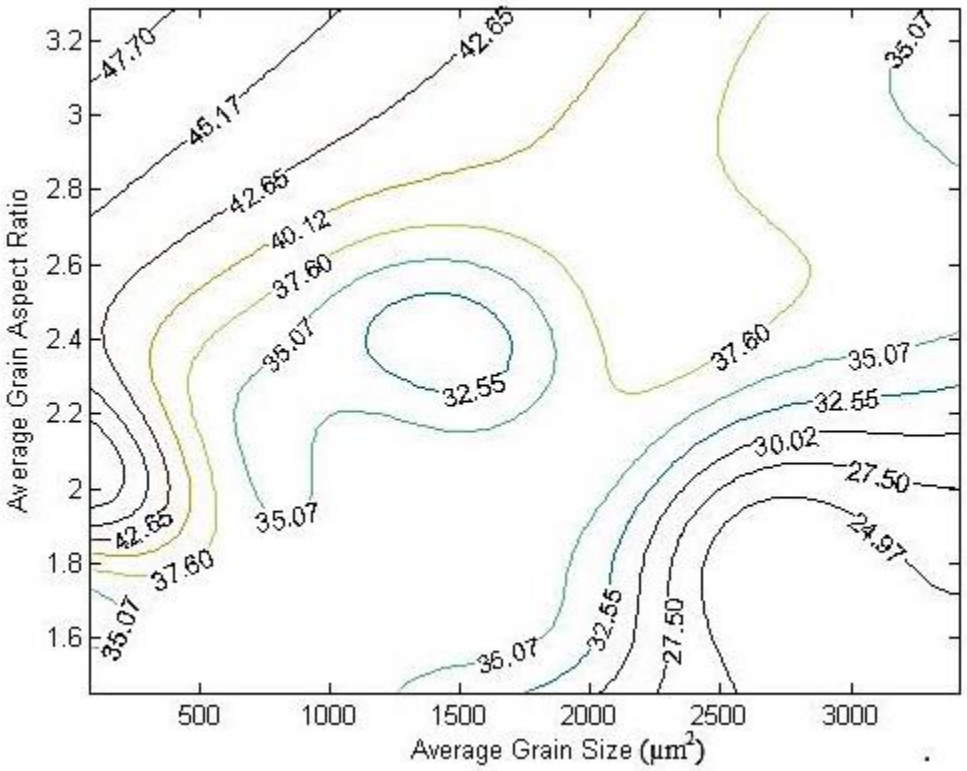

Figure 4.3. Contour plot of Kriging surrogate model for fracture strength as a function of average grain size and aspect ratio

The results indicate that in general Mg alloys with smaller average grain size and higher aspect ratio have higher fracture energy. These results are in good agreement with the work of Guo et al. [109] which indicates microstructures with finer grains have higher fracture toughness and strength. Moreover, it is shown that the manufacturing processes such as hot-rolling [117, 118] and annealing [116] which are utilized to increase the strength of the AZ31 magnesium alloy, decreases the grain size which causes property improvement. It has been also predictable that grains with higher aspect ratio increase the fracture strength since as it can be observed in Figure 4.2 grains hinder the crack propagation. Grains' aspect-ratio effect is more significant when the average grain size is small.

4.4.2. Material with Elliptical Inclusions

Many heterogeneous materials can be modeled by matrix with elliptical inclusions such as porous materials and fiber reinforced composites. Magnesium matrix composite processed by a gas-pressure infiltration in laboratories is an example of this type of materials. The processed composite is based on magnesium alloy reinforced with long Silicon Carbide fibers. This example focuses on the effect of orientation and aspect ratio of the aligned inclusions on the fracture strength of composite. The orientations are calculated in degree with respect to a horizontal line perpendicular to crack orientation. The volume fraction and cross section of the fibers are kept constant in all sample models to eliminate their possible effect on the performance function. Then, 50 models are generated based on Latin hypercube sampling approach [119], and analyzed using nonlinear finite element analysis by LS-DYNA software. Schematic of the model before crack propagation is depicted in Figure 4.4, and the surrogate model for this problem is also shown in Figure 4.5.

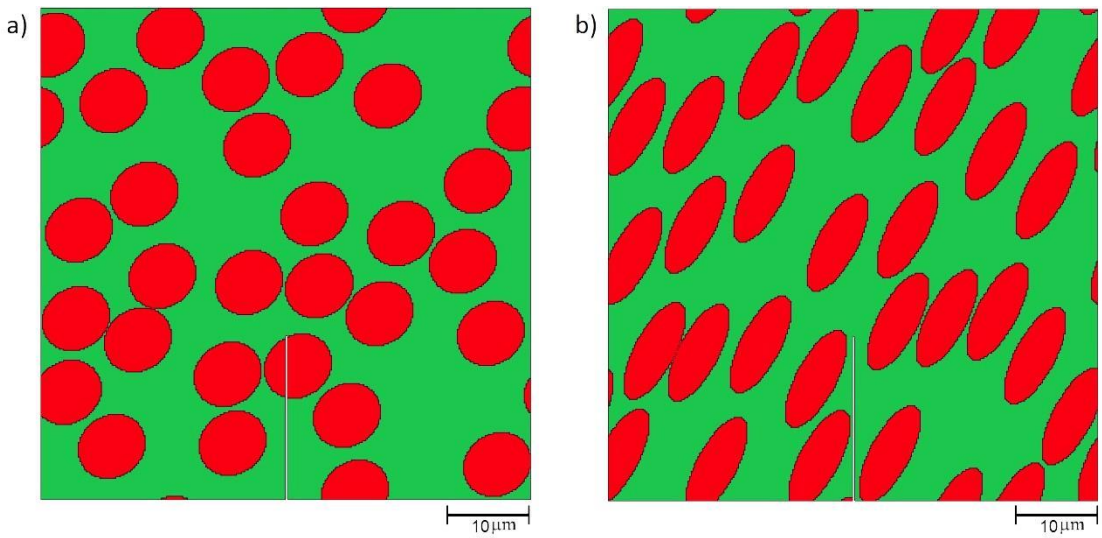

Figure 4.4. Schematic of models including elliptical inclusions: (a) aspect ratio of 1.15 and orientation of 34 degree and (b) aspect ratio of 2.72 and orientation of 62 degree

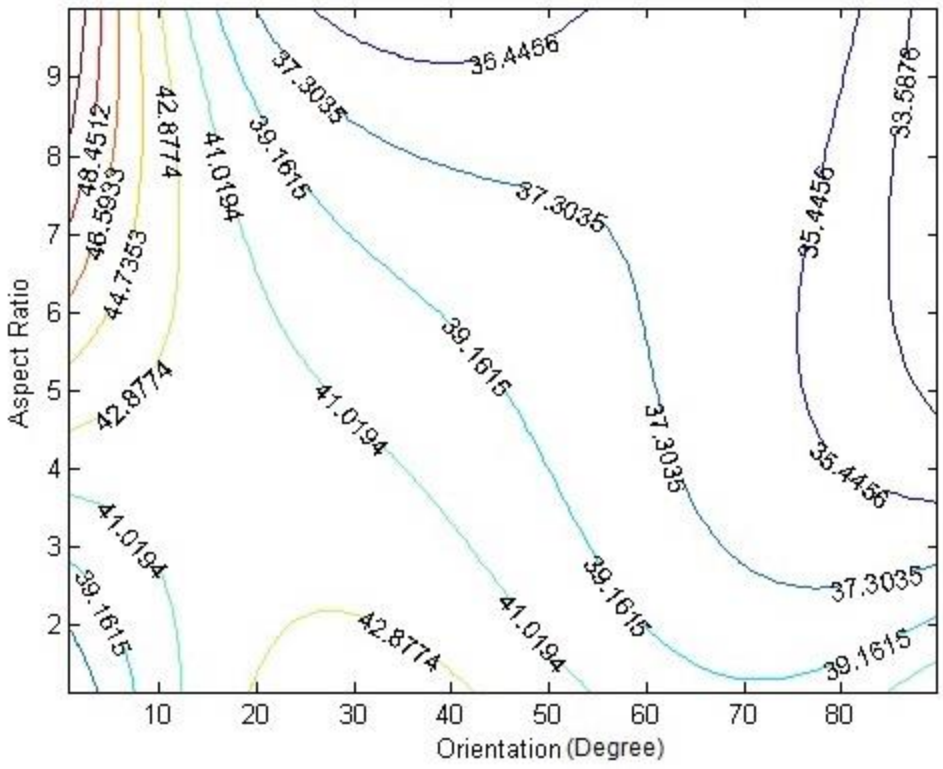

Figure 4.5. Contour plot of surrogate model for fracture strength as a function of orientation and aspect ratio

As it is illustrated by a surrogate model, the maximum fracture strength can be obtained when the inclusions oriented perpendicular to the crack propagation. This shows the hindering effect of inclusions in front of crack propagation. Similar to pervious example, the higher aspect ratio causes higher fracture strength due to the grains hindering effect for crack propagation when inclusions are perpendicular to initial crack. Therefore, increasing the aspect ratio of inclusions aligned perpendicular to the initial crack can effectively increase the fracture strength of material. On the contrary, the aspect ratio of the inclusions parallel to initial crack has opposite effect on the fracture strength since their extended interface zones along crack propagation are prone to failure. Henceforth, if the inclusions are oriented parallel to initial crack it is better to have circular fibers rather than elliptical fibers.

5. CONCLUSION

5.1. Summary and Discussion

This work represents the new material design framework which is currently in its infancy stages. It focuses on the design of microstructured materials as a key element in design framework. The microstructural information yields the variables of this optimization problem. The biggest challenge in extracting, quantifying, and utilizing this information is due to the high amount of randomness and complexity which inherently exists at the micro-scale of many materials. In order to overcome this challenge, statistical characterization and reconstruction methodologies have been incorporated. Although the statistical correlation functions are capable to convey the complex microstructural information, they are incapable to separate and cluster this information in a comprehensible way. While some researchers have attempted to find a relation between some physical features of a microstructure and its two point correlation function [82, 86, 89], still no clear and comprehensive relation has been established. In other words, the statistical correlation functions do not offer meaningful mappings to physical features and processing parameters. Alternatively, physical descriptor-based characterization has been proposed. The major advantage and strength of physical descriptors is their clear physical meanings which lead to meaningful mappings to processing parameters. These descriptors can be effectively utilized for heterogeneous microstructures consisting of phases with simple and regular geometric shapes, but they fail to describe media with random-shaped phases. They can just approximate some physical features and disregard many complex details which may be present in random microstructures. Therefore, there are some limitations in using these descriptors in practice as well as statistical characterization.

The link between microstructural information and bulk properties of material needs to be investigated through modeling and analysis. Depending on the describing parameters, different algorithms have been developed to reconstruct or generate a model. For instance, statistical reconstructions are based on optimization methodologies such as simulated annealing or genetic algorithm in which the objective is minimization of error between statistical correlation functions of target microstructure and the reconstructed model. The significant disadvantage of this modeling is its high computational cost. Moreover, since the statistical functions cannot offer meaningful mappings to processing parameters, it is not feasible to manufacture a sample material based on these functions. Therefore, physical-based reconstruction algorithms have been more successful in practice. For example, CA algorithm for grain growth which is based on recrystallization kinetics has been utilized for modeling alloys. The CA algorithm also provides the option of controlling some physical features such as average grain size, grain interphase thickness, and relative positions of the grains. These physical features can be controlled during the manufacturing process as well. For example, grain size in alloys can be controlled by annealing conditions [116]. However, the CA reconstructed model might fail to contain some microstructural information of actual material which can have a significant effect on its mechanical behavior. Thus, it becomes difficult to quantify the uncertainty of the results. The other reconstruction algorithm explained in this work can generate a model with matrix containing elliptical inclusions. It gives a rough estimation for random-shaped inclusions, but it can still offer a good model for many types of materials such as synthesis or natural fiber-reinforced composites. It also provides the option of controlling several physical features such as aspect ratio, size, and orientation distribution of inclusions along with their volume fraction.

The next step after creating a model based on microstructural information is the evaluation of the desired material properties. This evaluation can be done through several repeated experimental investigations or theoretical and numerical analysis. Although the experimental investigations provide the most reliable results, their costs and the amount of time required limit the practicality of experimental approaches. Hence, the numerical

analysis can be used instead of expensive experimental works. In this work, finite element software of LS-DYNA, which has been developed based on valid theoretical formulations, has been utilized to evaluate the mechanical behavior of microstructured models. Since the domain of each microstructural feature is continuous and infinite, it is unfeasible to search all the members of a domain to find the best possible solution. Thus, surrogate models have been created based on interpolation of several sample points to demonstrate the behavior of objective property or performance as a function of variable parameters which are microstructural features in this material framework. Then, based on the graphical approximation plot of objective function, the optimal points have been found. Finally, two sample examples have been solved through the aforementioned material design framework.

5.2. Recommendation for Future Research

In the course of this project, there are various areas which require further research. Future research opportunities are included in following list:

- The accuracy of results can be improved by extending the work to a three-dimensional finite element analysis. A serial sectioning process can be used to develop a three-dimensional (3D) representation of the microstructure. In addition, CA algorithm for 3D grain growth or 3D-statistical reconstruction approach can be utilized to generate material models for 3D finite element analysis.

- The relationship between processing parameters and microstructural information is an important aspect in material design framework which needs further comprehensive investigations. Without understanding the effect of different manufacturing processes and parameters involved in the process on the material's microstructure, there is no guarantee of manufacturability for designed material.

- More investigations are also required for development of material reconstruction methods. The fidelity of the models can be enhanced by improving the reconstruction algorithms. Developing a reconstructing algorithm based on the simulation of the manufacturing process is one approach to achieve high fidelity material models.

- The results of finite element analysis can be improved by developing better FE models with higher accuracy in the micro-scale level. For example, cohesive elements can be utilized instead of simple shell elements.

- The design problem can be improved by considering more microstructural characteristics as design variables. Moreover, multiple properties and performances can be considered as the objective functions of the optimization problem and solved through multi-functional optimization methods.

- The optimization search can be improved by developing algorithms which can enhance the fidelity of the surrogate model for better approximation.

LIST OF REFERENCES

LIST OF REFERENCES

[1] C. Bettles and M. Gibson, "Current wrought magnesium alloys: strengths and weaknesses," *Jom,* vol. 57, pp. 46-49, 2005.

[2] G. B. Olson, "Designing a new material world," *Science,* vol. 288, pp. 993-998, May 2000.

[3] D. L. McDowell, J. Panchal, H. J. Choi, C. Seepersad, J. Allen, and F. Mistree, *Integrated design of multiscale, multifunctional materials and products*: Butterworth-Heinemann, 2009.

[4] W. Bonfield, M. Rühle, H. Dosch, E. Mittemeijer, M. Van de voorde, Y. Bréchet, *et al.*, "European white book on fundamental research in materials science," *Max-Planck–Institut Für Metallforschung,* p. 72-85, 2001.

[5] A. T. Olewnik and K. E. Lewis, "On validating design decision methodologies," in ASME 2003 International Design Engineering Technical Conferences and Computers and Information in Engineering Conference, 2003, pp. 747-756.

[6] M. F. Ashby and K. Johnson, Materials and design: the art and science of material selection in product design: Butterworth-Heinemann, 2013.

[7] J. Arora, *Introduction to optimum design*: Academic Press, 2004.

[8] N. Dylla, "Thinking methods and procedures in mechanical design," *Mechanical design, technical university of Munich, PhD,* 1991.

[9] P. N. Koch, T. W. Simpson, J. K. Allen, and F. Mistree, "Statistical approximations for multidisciplinary design optimization: the problem of size," *Journal of Aircraft,* vol. 36, pp. 275-286, 1999.

[10] B. O'Sullivan, "Interactive constraint-aided conceptual design," *AI EDAM,* vol. 16, pp. 303-328, 2002.

[11] C. C. Seepersad, B. Dempsey, J. K. Allen, F. Mistree, and D. L. McDowell, "Design of multifunctional honeycomb materials," *AIAA journal,* vol. 42, pp. 1025-1033, 2004.

[12] J. Panchal, C. Paredis, J. Allen, and F. Mistree, "Design process simplification via scale and decision decoupling—a vale of information based approach," *J. Computing and Information Sciences in Engineering, 9 (2), pp. 21-51,* vol. 12, 2009.

[13] J. H. Panchal, H.-J. Choi, J. Shephard, J. K. Allen, D. L. McDowell, and F. Mistree, "A strategy for simulation-based multiscale, multi-functional products and associated design processes," in *ASME 2005 International Design Engineering Technical Conferences and Computers and Information in Engineering Conference*, 2005, pp. 845-857.

[14] J. Cagan, M. I. Campbell, S. Finger, and T. Tomiyama, "A framework for computational design synthesis: model and applications," *Journal of Computing and Information Science in Engineering,* vol. 5, pp. 171-181, 2005.

[15] M. E. Eberhart and D. P. Clougherty, "Looking for design in materials design," *Nature materials,* vol. 3, pp. 659-661, 2004.

[16] S. Torquato, *Random heterogeneous materials: microstructure and macroscopic properties* vol. 16. New York, NY, USA: Springer Science + Business Media, 2002.

[17] K. Z. Chen and X. A. Feng, "Computer-aided design method for the components made of heterogeneous materials," *Computer-aided design,* vol. 35, pp. 453-466, 2003.

[18] S. Torquato, "Optimal design of heterogeneous materials," *Annual Review of Materials Research* vol. 40, pp. 101-129, 2010.

[19] W. K. Liu and C. McVeigh, "Predictive multiscale theory for design of heterogeneous materials," *Computational Mechanics,* vol. 42, pp. 147-170, 2008.

[20] W. Voigt, "Ueber die Beziehung zwischen den beiden elasticitätsconstanten isotroper körper," *Annalen der Physik,* vol. 274, pp. 573-587, 1889.

[21] A. Reuss, "Berechnung der fließgrenze von mischkristallen auf grund der plastizitätsbedingung für einkristalle," *ZAMM - Journal of Applied Mathematics and Mechanics / Zeitschrift für Angewandte Mathematik und Mechanik,* vol. 9, pp. 49-58, 1929.

[22] J. Mackenzie, "The elastic constants of a solid containing spherical holes," *Proceedings of the Physical Society. Section B,* vol. 63, p. 2-19, 1950.

[23] E. Kröner, "Computation of the elastic constants of polycrystals from constants of single crystals," *Z. Phys,* vol. 151, pp. 504-518, 1958.

[24] R. Hill, "A self-consistent mechanics of composite materials," *Journal of the Mechanics and Physics of Solids,* vol. 13, pp. 213-222, 1965.

[25] J. D. Eshelby, "The determination of the elastic field of an ellipsoidal inclusion, and related problems," *Proceedings of the Royal Society of London. Series A. Mathematical and Physical Sciences,* vol. 241, pp. 376-396, 1957.

[26] J. Eshelby, "Elastic inclusions and inhomogeneities," *Progress in solid mechanics,* vol. 2, pp. 89-140, 1961.

[27] K. Z. Markov, "Elementary micromechanics of heterogeneous media," in *Heterogeneous media,* ed: Springer, 2000, pp. 1-162.

[28] G. B. Olson, "Computational design of hierarchically structured materials," *Science,* vol. 277, pp. 1237-1242, 1997.

[29] N. Otsu, "A threshold selection method from gray-level histograms," *IEEE Transactions on Systems, Man and Cybernetics,* vol. 9, pp. 62-66, 1979.

[30] K. Sobczyk and D. J. Kirkner, *Stochastic Modeling of Microstructures*. New York: Springer, 2001.

[31] A. Al-Ostaz, A. Diwakar, and K. I. Alzebdeh, "Statistical model for characterizing random microstructure of inclusion–matrix composites," *Journal of Materials Science,* vol. 42, pp. 7016-7030, 2007.

[32] D. Jeulin, "Random texture models for material structures," *Statistics and Computing,* vol. 10, pp. 121-132, 2000.

[33] G. Steel, "The two-point correlation function and the specific heat," *Physics Letters A,* vol. 27, pp. 550-551, 1968.

[34] S. C. Blair, P. A. Berge, and J. G. Berryman, "Using two-point correlation functions to characterize microgeometry and estimate permeabilities of sandstones and porous glass," *Journal of Geophysical Research: Solid Earth,* vol. 101, pp. 20359-20375, 1996.

[35] G. Saheli, H. Garmestani, and B. L. Adams, "Microstructure design of a two phase composite using two-point correlation functions," *Journal of Computer-Aided Materials Design,* vol. 11, pp. 103-115, 2004.

[36] A. Gokhale and H. Singh, "Computer Simulations of realistic microstructures using statistical two-point correlation functions," *Microscopy and Microanalysis,* vol. 11, pp. 1632-1633, 2005.

[37] A. M. Gokhale, A. Tewari, and H. Garmestani, "Constraints on microstructural two-point correlation functions," *Scripta Materialia,* vol. 53, pp. 989-993, 2005.

[38] G. Jefferson, H. Garmestani, R. Tannenbaum, A. Gokhale, and E. Tadd, "Two-point probability distribution function analysis of Co-polymer nano-composites," *International Journal of Plasticity,* vol. 21, pp. 185-198, 2005.

[39] D. S. Li, G. Saheli, M. Khaleel, and H. Garmestani, "Quantitative prediction of effective conductivity in anisotropic heterogeneous media using two-point correlation functions," *Computational Materials Science,* vol. 38, pp. 45-50, 2006.

[40] S. Torquato, "Necessary conditions on realizable two-point correlation functions of random media," *Industrial and Engineering Chemistry Research,* vol. 45, pp. 6923-6928, 2006.

[41] Y. Jiao, F. H. Stillinger, and S. Torquato, "Modeling heterogeneous materials via two-point correlation functions: basic principles," *Physical Review E - Statistical, Nonlinear, and Soft Matter Physics,* vol. 76, 2007.

[42] Y. Jiao, F. H. Stillinger, and S. Torquato, "Modeling heterogeneous materials via two-point correlation functions. II. Algorithmic details and applications," *Physical Review E,* vol. 77, p. 031135, 2008.

[43] A. Belvin, R. Burrell, A. Gokhale, N. Thadhani, and H. Garmestani, "Application of two-point probability distribution functions to predict properties of heterogeneous two-phase materials," *Materials Characterization,* vol. 60, pp. 1055-1062, 2009.

[44] M. Baniassadi, H. Garmestani, D. S. Li, S. Ahzi, M. Khaleel, and X. Sun, "Three-phase solid oxide fuel cell anode microstructure realization using two-point correlation functions," *Acta Materialia,* vol. 59, pp. 30-43, 2011.

[45] H. L. Frisch and F. H. Stillinger, "Contribution to the statistical geometric basis of radiation scattering," *The Journal of Chemical Physics,* vol. 38, pp. 2200-2207, 1963.

[46] P. Debye, H. R. Anderson, and H. Brumberger, "Scattering by an Inhomogeneous solid. ii. the correlation function and its application," *Journal of Applied Physics,* vol. 28, pp. 679-683, 1957.

[47] J. G. Berryman, "Relationship between specific surface area and spatial correlation functions for anisotropic porous media," *Journal of Mathematical Physics,* vol. 28, pp. 244-245, 1987.

[48] C. J. Gommes, Y. Jiao, and S. Torquato, "Microstructural degeneracy associated with a two-point correlation function and its information content," *Physical Review E,* vol. 85, p. 051140, 2012.

[49] M. Doi, "A new variational approach to the diffusion and the flow problem in porous media," *Journal of the Physical Society of Japan,* vol. 40, pp. 567-572, 1976.

[50] J. Rubinstein and J. B. Keller, "Lower bounds on permeability," *Physics of Fluids (1958-1988),* vol. 30, pp. 2919-2921, 1987.

[51] J. Rubinstein and S. Torquato, "Diffusion-controlled reactions: Mathematical formulation, variational principles, and rigorous bounds," *The Journal of Chemical Physics,* vol. 88, pp. 6372-6380, 1988.

[52] B. Lu and S. Torquato, "Lineal-path function for random heterogeneous materials," *Physical Review A,* vol. 45, pp. 922-929, 1992.

[53] S. N. Chiu, D. Stoyan, W. S. Kendall, and J. Mecke, *Stochastic Geometry and Its Applications*: Wiley, 2013.

[54] G. Matheron, Random Sets and Integral Geometry: Wiley, 1975.

[55] S. Torquato and B. Lu, "Chord-length distribution function for two-phase random media," *Physical Review E,* vol. 47, pp. 2950-2953, 1993.

[56] E. E. Underwood, *Quantitative Stereology*: Addison-Wesley Pub. Co., 1970.

[57] F. G. Ho and W. Strieder, "Asymptotic expansion of the porous medium, effective diffusion coefficient in the Knudsen number," *The Journal of Chemical Physics,* vol. 70, pp. 5635-5639, 1979.

[58] T. K. Tokunaga, "Porous media gas diffusivity from a free path distribution model," *The Journal of Chemical Physics,* vol. 82, pp. 5298-5299, 1985.

[59] M. Tassopoulos and D. E. Rosner, "Simulation of vapor diffusion in anisotropic particulate deposits," *Chemical Engineering Science,* vol. 47, pp. 421-443, 1992.

[60] A. H. Thompson, A. J. Katz, and C. E. Krohn, "The microgeometry and transport properties of sedimentary rock," *Advances in Physics,* vol. 36, pp. 625-694, 1987.

[61] S. Prager, "Diffusion and viscous flow in concentrated suspensions," *Physica,* vol. 29, pp. 129-139, 1963.

[62] S. Torquato, "Statistical description of microstructures," *Annual Review of Materials Research,* vol. 32, pp. 77-111, 2002.

[63] S. Torquato, J. D. Beasley, and Y. C. Chiew, "Two-point cluster function for continuum percolation," *The Journal of Chemical Physics,* vol. 88, pp. 6540-6547, 1988.

[64] P. Hertz, "Über den gegenseitigen durchschnittlichen Abstand von Punkten, die mit bekannter mittlerer Dichte im Raume angeordnet sind," *Mathematische Annalen,* vol. 67, pp. 387-398, 1909.

[65] J. B. Keller, L. A. Rubenfeld, and J. E. Molyneux, "Extremum principles for slow viscous flows with applications to suspensions," *Journal of Fluid Mechanics,* vol. 30, pp. 97-125, 1967.

[66] J. L. Finney, "Random packings and the structure of simple liquids. I. The geometry of random close packing," *Proceedings of the Royal Society of London. Series A, Mathematical and Physical Sciences,* vol. 319, pp. 479-493, 1970.

[67] J. G. McNally and E. C. Cox, "Spots and stripes: the patterning spectrum in the cellular slime mould Polysphondylium pallidum," *Development,* vol. 105, pp. 323-333, 1989.

[68] R. Zallen, "Amorphous Morphology: The Geometry and Topology of Disorder," in *The Physics of Amorphous Solids*, ed: Wiley-VCH Verlag GmbH, 2007, pp. 33-85.

[69] S. Torquato, B. Lu, and J. Rubinstein, "Nearest-neighbor distribution functions in many-body systems," *Physical Review A,* vol. 41, pp. 2059-2075, 1990.

[70] H. Reiss, H. L. Frisch, and J. L. Lebowitz, "Statistical mechanics of rigid spheres," *The Journal of Chemical Physics,* vol. 31, pp. 369-380, 1959.

[71] D. J. Vezzetti, "A new derivation of some fluctuation theorems in statistical mechanics," *Journal of Mathematical Physics,* vol. 16, pp. 31-33, 1975.

[72] R. M. Ziff, "On the bulk distribution functions and fluctuation theorems," *Journal of Mathematical Physics,* vol. 18, pp. 1825-1831, 1977.

[73] T. M. Truskett, S. Torquato, and P. G. Debenedetti, "Density fluctuations in many-body systems," *Physical Review E,* vol. 58, pp. 7369-7380, 1998.

[74] B. Lu and S. Torquato, "Nearest-surface distribution functions for polydispersed particle systems," *Physical Review A,* vol. 45, pp. 5530-5544, 1992.

[75] S. Torquato and G. Stell, "Microstructure of two-phase random media. III. The n-point matrix probability functions for fully penetrable spheres," *The Journal of Chemical Physics,* vol. 79, pp. 1505-1510, 1983.

[76] S. Torquato and F. Lado, "Characterisation of the microstructure of distributions of rigid rods and discs in a matrix," *Journal of Physics A: Mathematical and General,* vol. 18, p. 141, 1985.

[77] S. Torquato, "Interfacial surface statistics arising in diffusion and flow problems in porous media," *The Journal of Chemical Physics,* vol. 85, pp. 4622-4628, 1986.

[78] G. Stell and P. A. Rikvold, "Polydispersity in fluids and composites: Some theoretical results," *International Journal of Thermophysics,* vol. 7, pp. 863-876, 1986.

[79] C. A. Miller and S. Torquato, "Diffusion-controlled reactions among spherical traps: Effect of polydispersity in trap size," *Phys Rev B Condens Matter,* vol. 40, pp. 7101-7108, Oct. 1989.

[80] B. Lu and S. Torquato, "Lineal-path function for random heterogeneous materials. II. Effect of polydispersivity," *Physical Review A,* vol. 45, pp. 7292-7301, 1992.

[81] B. Lu and S. Torquato, "General formalism to characterize the microstructure of polydispersed random media," *Physical Review A,* vol. 43, pp. 2078-2080, 1991.

[82] C. L. Y. Yeong and S. Torquato, "Reconstructing random media," *Physical Review E,* vol. 57, pp. 495-506, 1998.

[83] P. Debye and A. M. Bueche, "Scattering by an Inhomogeneous Solid," *Journal of Applied Physics,* vol. 20, pp. 518-525, 1949.

[84] P. B. Corson, "Correlation functions for predicting properties of heterogeneous materials. III. Effective elastic moduli of two-phase solids," *Journal of Applied Physics,* vol. 45, pp. 3171-3179, 1974.

[85] H. Garmestani, S. Lin, B. L. Adams, and S. Ahzi, "Statistical continuum theory for large plastic deformation of polycrystalline materials," *Journal of the Mechanics and Physics of Solids,* vol. 49, pp. 589-607, 2001.

[86] Y. Liu, M. Steven Greene, W. Chen, D. A. Dikin, and W. K. Liu, "Computational microstructure characterization and reconstruction for stochastic multiscale material design," *Computer-Aided Design,* vol. 45, pp. 65-76, 2013.

[87] V. Sundararaghavan and A. Kumar, "Probabilistic modeling of microstructure evolution using finite element representation of statistical correlation functions," *International Journal of Plasticity,* vol. 30–31, pp. 62-80, 2012.

[88] S. Torquato, "Necessary conditions on realizable two-point correlation functions of random media," *Industrial & Engineering Chemistry Research,* vol. 45, pp. 6923-6928, 2006.

[89] H. Xu, Y. Li, C. Brinson, and W. Chen, "A descriptor-based design methodology for developing heterogeneous microstructural materials system," *Journal of Mechanical Design,* vol. 136, pp. 51-67, 2014.

[90] Y. Jiaoa, F. H. Stillingerb, and S. Torquato, "A superior descriptor of random textures and its predictive capacity," *Proceedings of the National Academy of Sciences,* 2009.

[91] M. S. Talukdar, O. Torsaeter, and M. A. Ioannidis, "Stochastic reconstruction of particulate media from two-dimensional images," *Journal of Colloid and Interface Science,* vol. 248, pp. 419-428, 2002.

[92] N. C. Kumar, K. Matouš, and P. H. Geubelle, "Reconstruction of periodic unit cells of multimodal random particulate composites using genetic algorithms," *Computational Materials Science,* vol. 42, pp. 352-367, 2008.

[93] W. Aspray and A. Burks, Papers of John Von Neumann on computing and computer theory, Vol 12: MIT Press, 1986.

[94] S. Wolfram, "Theory and Applications of Cellular Automata, Advanced Series on Complex Systems, Selected Papers 1983–1986", Vol. 1, *Singapore: World Sci,* 1986.

[95] H. Won Lee and Y. T. Im, "Numerical modeling of dynamic recrystallization during nonisothermal hot compression by cellular automata and finite element analysis," *International Journal of Mechanical Sciences,* vol. 52, pp. 1277-1289, 2010.

[96] S. Das, "Modeling mixed microstructures using a multi-level cellular automata finite element framework," *Computational Materials Science,* vol. 47, pp. 705-711, 2010.

[97] H. Hallberg, M. Wallin, and M. Ristinmaa, "Simulation of discontinuous dynamic recrystallization in pure Cu using a probabilistic cellular automaton," *Computational Materials Science,* vol. 49, pp. 25-34, 2010.

[98] S. Ghosh, P. Gabane, A. Bose, and N. Chakraborti, "Modeling of recrystallization in cold rolled copper using inverse cellular automata and genetic algorithms," *Computational Materials Science,* vol. 45, pp. 96-103, 2009.

[99] B. Derby and M. Ashby, "On dynamic recrystallisation," *Scripta Metallurgica,* vol. 21, pp. 879-884, 1987.

[100] E. Nes, N. Ryum, and O. Hunderi, "On the Zener drag," *Acta Metallurgica,* vol. 33, pp. 11-22, 1985.

[101] R. Doherty, D. Hughes, F. Humphreys, J. Jonas, D. J. Jensen, M. Kassner, *et al.*, "Current issues in recrystallization: a review," *Materials Science and Engineering: A,* vol. 238, pp. 219-274, 1997.

[102] D. Raabe, "Mesoscale simulation of spherulite growth during polymer crystallization by use of a cellular automaton," *Acta Materialia,* vol. 52, pp. 2653-2664, 2004.

[103] Y. Liu, T. Baudin, and R. Penelle, "Simulation of normal grain growth by cellular automata," *Scripta Materialia,* vol. 34, pp. 1679-1683, 1996.

[104] S. Raghavan and S. S. Sahay, "Modeling the grain growth kinetics by cellular automaton," *Materials Science and Engineering: A,* vol. 445, pp. 203-209, 2007.

[105] S. Raghavan and S. S. Sahay, "Modeling the topological features during grain growth by cellular automaton," *Computational Materials Science,* vol. 46, pp. 92-99, 2009.

[106] M. Tschopp, G. Wilks, and J. Spowart, "Multi-scale characterization of orthotropic microstructures," *Modelling and Simulation in Materials Science and Engineering,* vol. 16, p. 065009, 2008.

[107] J. E. Smith and M. L. Jordan, "Mathematical and graphical interpretation of the log-normal law for particle size distribution analysis," *Journal of Colloid Science,* vol. 19, pp. 549-559, 1964.

[108] O. G. Raabe, "Particle size analysis utilizing grouped data and the log-normal distribution," *Journal of Aerosol Science,* vol. 2, pp. 289-303, 1971.

[109] X. Guo, K. Chang, L. Q. Chen, and M. Zhou, "Determination of fracture toughness of AZ31 Mg alloy using the cohesive finite element method," *Engineering Fracture Mechanics,* vol. 96, pp. 401-415, 2012.

[110] G. L. Harris, *Properties of silicon carbide*: Iet, 1995.

[111] G. Shi, "Chapter 8 - Kriging," in *Data Mining and Knowledge Discovery for Geoscientists,* G. Shi, Ed., ed Oxford: Elsevier, 2014, pp. 238-274.

[112] H. B. Nielsen and K. F. Thuesen, "Kriging and radial basis functions," *IMM, Technical University of Denmark, Kongens Lyngby, Denmark,* 2005.

[113] S. Lophaven, H. Nielsen, and J. Sondergaard, "DACE—A Matlab Kriging Toolbox, Version 2, informatics and mathematical modelling," *Technical University of Denmark,* 2002.

[114] O. Duygulu and S. R. Agnew, "The effect of temperature and strain rate on the tensile properties of textured magnesium alloy AZ 31 B sheet," in *Magnesium Technology 2003 as held at the 2003 TMS Annual Meeting,* 2003, pp. 237-242.

[115] H. Somekawa and T. Mukai, "Fracture toughness in Mg–Al–Zn alloy processed by equal-channel-angular extrusion," *Scripta Materialia*, vol. 54, pp. 633-638, 2006.

[116] A. Yamamoto, M. Kakishiro, M. Ikeda, and H. Tsubakino, "Grain refinement on AZ31 manesium alloy by highly strained and annealed method," in *Materials Science Forum*, vol. 449, pp. 669-672, 2004.

[117] Q. Miao, L. X. Hu, H. F. Sun, and E. D. Wang, "Grain refining and property improvement of AZ31 Mg alloy by hot rolling," *Transactions of Nonferrous Metals Society of China*, vol. 19, Supplement 2, pp. s326-s330, 2009.

[118] E. Essadiqi, M. T. Shehata, A. Javaid, C. Galvani, G. Shen, S. Yue, *et al.*, "Microstructure and temperature monitoring during the hot rolling of AZ31," *Jom*, vol. 61, pp. 25-28, 2009.

[119] M. D. McKay, R. J. Beckman, and W. J. Conover, "A comparison of three methods for selecting values of input variables in the analysis of output from a computer code," *Technometrics*, vol. 42, pp. 55-61, 2000.